JOURNAL OF GEOPHYSICAL RESEARCH, VOL. 108, NO. B9, 2450, doi:10.1029/2002JB002241, 2003

Crustal velocity field of Mexico from continuous GPS measurements, 1993 to June 2001: Implications for the neotectonics of Mexico

Bertha Márquez-Azúa
Departamento de Geografía y Ordenación Territorial, Universidad de Guadalajara, Guadalajara, Jalisco, Mexico

Charles DeMets
Department of Geology and Geophysics, University of Wisconsin-Madison, Madison, Wisconsin, USA

Received 11 October 2002; revised 9 June 2003; accepted 20 June 2003; published 27 September 2003.

[1] We combine velocities for 14 continuous GPS stations spanning Mexico and 173 additional continuous GPS sites on the North American and Pacific plates to study the large-scale deformation of Mexico. The new station velocities, which are derived from more than 6000 days of previously unused GPS data, provide the first ever view of the crustal velocity field of Mexico. Key results are as follows: (1) Areas north of the Mexican Volcanic Belt, not including Baja California, move with the North American plate interior within the 1–2 mm yr^{-1} station velocity uncertainties. Station velocities for the Mexican Basin and Range are consistent with no present-day extension and yield an upper 95% limit of 1–3 mm yr^{-1} for any regional extension. (2) South of the Mexican Volcanic Belt, five of the six sites move significantly relative to the North American plate. All sites in the Yucatan Peninsula move toward the east at 3–4 mm yr^{-1}, possibly defining an independent Yucatan block. (3) Site velocities are consistent with limits of 0–4 mm yr^{-1} for present slip across the Mexican Volcanic Belt. (4) Tampico, on the gulf coast, exhibits eastward motion consistent with gravity sliding known to occur in the adjacent Mexican Ridges fold belt. (5) Southeastward motion of La Paz relative to the Pacific plate is consistent with the hypothesis that the Baja Peninsula is not fully attached to the Pacific plate. (6) Residual velocities for 160 North American plate GPS stations outside of Mexico exhibit no coherent regional patterns indicative of internal plate deformation. *INDEX TERMS:* 1206 Geodesy and Gravity: Crustal movements—interplate (8155); 1208 Geodesy and Gravity: Crustal movements—intraplate (8110); 8107 Tectonophysics: Continental neotectonics; 8150 Tectonophysics: Plate boundary–general (3040); 8155 Tectonophysics: Plate motions–general; *KEYWORDS:* Mexico, neotectonics, Basin-and-Range, Mexican Volcanic Belt

Citation: Márquez-Azúa, B., and C. DeMets, Crustal velocity field of Mexico from continuous GPS measurements, 1993 to June 2001: Implications for the neotectonics of Mexico, *J. Geophys. Res.*, *108*(B9), 2450, doi:10.1029/2002JB002241, 2003.

1. Introduction

[2] The country of Mexico has one of the most remarkable tectonic settings on Earth. Mexico incorporates parts of the Pacific, North American, and Caribbean plates (Figure 1) and accommodates northeastward subduction of the Rivera and Cocos plates beneath a 1500-km-long stretch of its Pacific coast. In addition, the country is bisected by the Mexican Volcanic Belt, which extends east-southeastward across Mexico for more than 1000 km above the 80–100 km depth contour of the subducting Rivera and Cocos plates [*Pardo and Suarez*, 1995]. Earthquakes associated with the faults that separate these five tectonic plates, as well as earthquakes and volcanism within the volcanic belt constitute significant natural hazards to much of central and southern Mexico, including Mexico City, the heavily populated political and economic heart of the country.

[3] Despite the abundance of neotectonic problems posed by the juxtaposition of these five tectonic plates, studies of Mexican neotectonics that employ Global Positioning System (GPS) technology have been limited primarily to Baja California and a few areas of the Pacific coast. As a consequence, important questions about the large-scale crustal deformation of Mexico are still unanswered. These include whether lithosphere in northern Mexico is part of the stable interior of the North American plate or instead accommodates extension across Basin and Range structures north of the Mexican Volcanic Belt [*Henry and Aranda-Gomez*, 1992], and whether faults within the Mexican

0148-0227/03/2002JB002241$09.00

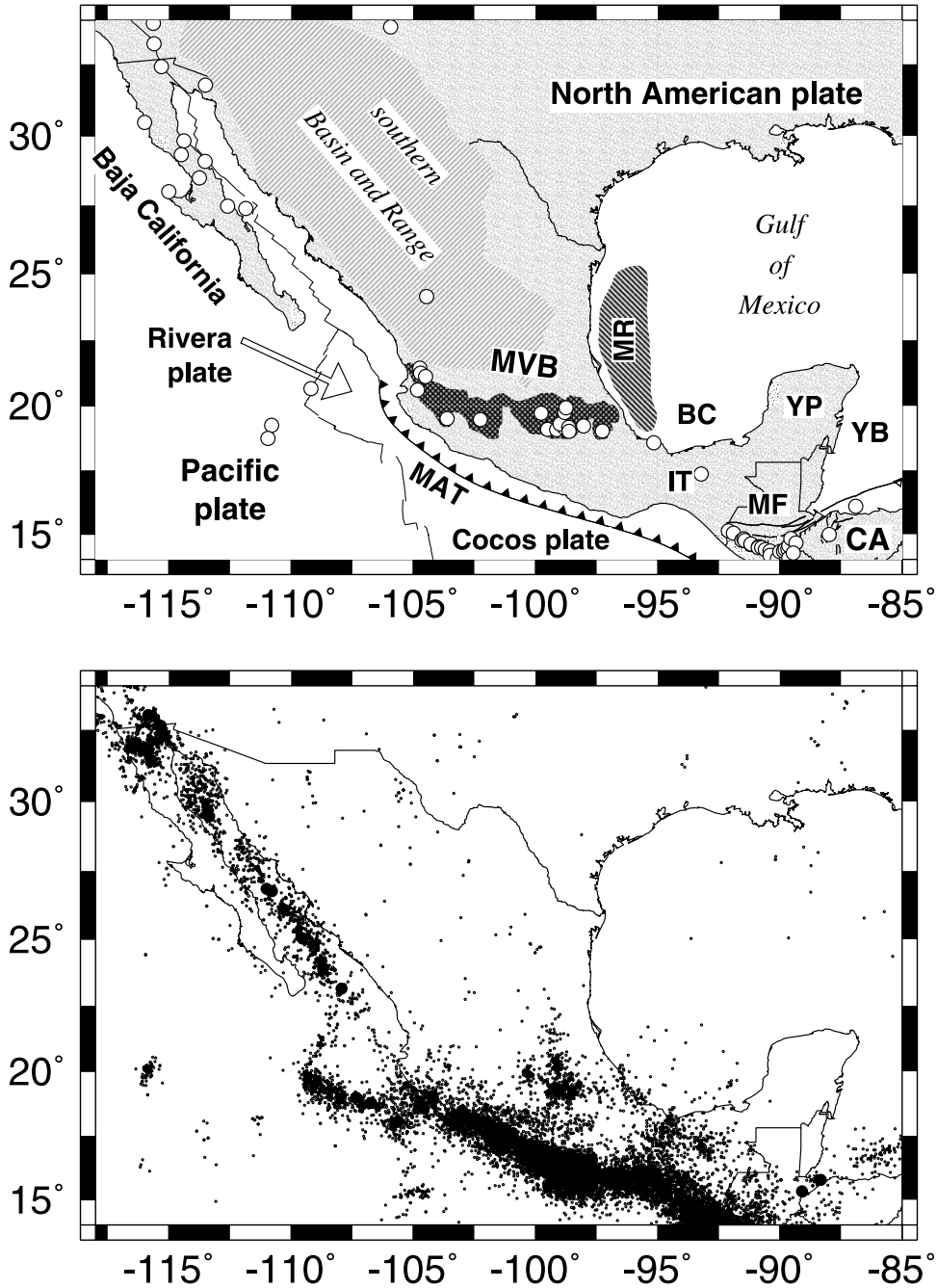

Figure 1. (top) Volcanotectonic setting of Mexico. Circles show locations of Quaternary volcanic eruptions. Limits of the southern Basin and Range province shown in this and subsequent Figures are defined by *Stewart et al.* [1998]. BC, Bay of Campeche; CA, Caribbean plate; IT, Isthmus of Tehuantepec; MAT, Middle America trench; MR, Mexican Ridges; MF, Motagua fault; MVB, Mexican Volcanic Belt; YB, Yucatan basin; YP, Yucatan Peninsula. (bottom) Small and large circles show earthquake epicenters with respective magnitudes of $m_b < 6.5$ and $m_b \geq 6.5$ and depths above 60 km reported by U.S. Geological Survey for the period 1963–2002 and earthquakes of all magnitudes above depths of 30 km reported by the Mexican National Seismic Network for the period 1974–2001.

Volcanic Belt accommodate significant present-day displacement. Detailed structural studies of the more than 50 faults within the Mexican Volcanic Belt that displace rocks of Quaternary age suggest that the bulk Neogene motion across the volcanic belt has been limited to NNW-SSE oriented extension of 0.2 ± 0.05 mm yr^{-1} [*Suter et al.*, 2001]. In contrast, some paleomagnetic and structural observations suggest that the volcanic belt is a locus of sinistral, transtensional slip [e.g., *Pasquaré et al.*, 1988; *Urrutia-Fucugauchi and Böhnel*, 1988; *Johnson and Harrison*, 1990; *Ferrari et al.*, 1994; *Soler-Archalde and Urrutia-Fucugauchi*, 1994].

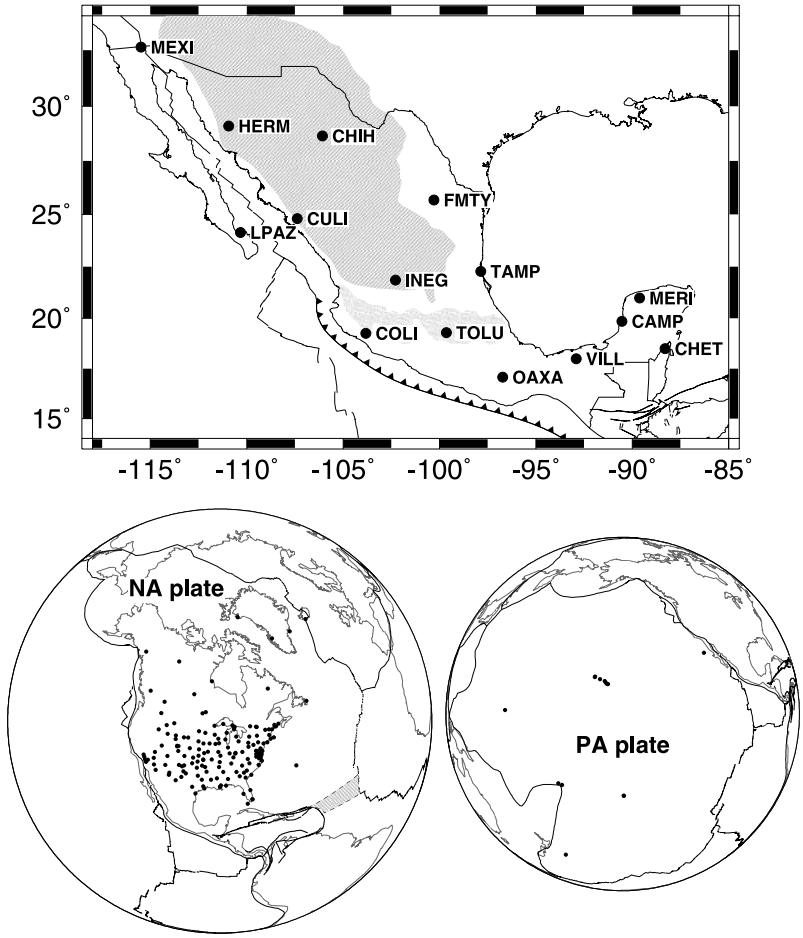

Figure 2. (top) Locations and names of RGNA GPS sites. (bottom) Locations of continuous GPS sites on (left) North American plate and (right) Pacific plate used for this analysis.

[4] Since early 1993, the Mexican government agency Instituto Nacional de Estadística, Geografía, e Informática (INEGI) has operated a nationwide network of 15 continuous GPS receivers (Figure 2) to provide first-order geodetic control and differential positioning throughout Mexico. The archive of GPS data from the Red Geodésica Nacional Activa (translated as the national active geodetic network and hereafter referred to as RGNA) is one of the oldest continuous GPS archives available for any country. Surprisingly, only a fraction of these data have been analyzed or used for geophysical studies, primarily due to difficulties in procuring the data from the archive and their cost (~$20 U.S. per station day).

[5] Following protracted legal negotiations for no-cost access to the RGNA data, we have procured and analyzed data from all 15 sites for 1993 to June 2001. Herein, we use GPS velocities for 14 of the 15 sites in the INEGI RGNA network to treat each of the above questions. Results for the remaining site (COLI) are reported by *Márquez-Azúa et al.* [2002] and are not repeated here. Ten of the RNGA stations are located far from active faults and are thus well suited for quantifying large-scale block motions in Mexico. The remaining sites are located close enough to active fault zones to be influenced by elastic strain associated with frictional locking of those faults. Our analysis thus consists partly of a description of the large-scale kinematics of Mexico and partly of an interpretation of individual site velocities, which provide varying degrees of useful information about motion along nearby faults.

2. Data

2.1. INEGI GPS Data

[6] The INEGI RGNA network presently consists of 15 continuous GPS stations that span Mexico (Figure 2 and Table 1). Fourteen of these sites began operating in February–April 1993, and one station, located in Campeche (CAMP), began operating in September 1995. Ashtech LM-XII3 receivers and antennas have operated continuously at 14 of the 15 sites since 1993, the lone exception being Aguascalientes (INEG), where a Trimble 4700 receiver and choke ring antenna replaced the original Ashtech LM XII-3 and antenna in early February 2000. Antennas at nine of the sites remained undisturbed on their original mounts during the entire period of observations. The antennas at five sites (CAMP, COLI, FMTY, HERM, and VILL) were moved once to new locations, and the antenna at CHIH was moved twice. Geodetic ties between the old and new antenna locations are not available. The network was not designed for geophysical purposes, hence the antennas are mounted on buildings, typically of modern concrete construction. Of the six sites we have visited, we

Table 1. RGNA Station Information[a]

Site	Cartesian Coordinates, m			Geodetic Coordinates		
	X	Y	Z	Latitude, °N	Longitude, °E	Height, m
Aguascalientes (INEG)	−1260435.700	−5788547.630	2360340.251	21.8561539	−102.2842024	1889.382
Campeche (CAMP)	−56581.307	−6001449.596	2151509.148	19.8444271	−90.5401652	13.210
Chetumal (CHET)	179584.806	−6048080.711	2010447.345	18.4952766	−88.2992242	4.002
Chihuahua (CHIH)	−1552307.732	−5382771.933	3041779.785	28.6621931	−106.0867388	1414.145
Culiacán (CULI)	−1730936.667	−5528855.273	2658865.646	24.7985526	−107.3839422	76.420
Monterrey (FMTY)	−1029483.408	−5657637.246	2750926.126	25.7155069	−100.3129053	522.751
Hermosillo (HERM)	−1996003.902	−5208674.530	3082959.590	29.0925473	−110.9672144	187.950
La Paz (LPAZ)	−2022283.132	−5461274.376	2592316.981	24.1387967	−110.3193442	−5.833
Mérida (MERI)	39480.823	−5957733.126	2269335.111	20.9800453	−89.6203168	8.885
Mexicali (MEXI)	−2312590.799	−4853743.769	3419740.382	32.6329907	−115.4757014	−21.446
Oaxaca (OAXA)	−713745.376	−6058204.974	1861815.243	17.0804557	−96.7193085	1606.878
Tampico (TAMP)	−807922.595	−5849358.283	2402967.696	22.2783211	−97.8640265	22.076
Toluca (TOLU)	−1008730.734	−5939707.396	2094568.114	19.2901702	−99.6384867	2650.199
Villahermosa (VILL)	−310300.603	−6060324.050	1957383.592	17.9904105	−92.9310978	28.772

[a]Cartesian site coordinates are specified in ITRF2000. Geodetic coordinates are relative to WGS-84 reference ellipsoid. Site epoch is 1 January 2000 except for VILL, for which the epoch is 1 January 2001. The coordinates for CAMP, CHIH, FMTY, HERM, and VILL are for antennas that were relocated to nearby alternative sites CAM2, CHI3, MTY2, HER2, and VIL2.

observed that the antennas have unobstructed sky views and are carefully mounted on ∼2-m-high concrete pillars located above the main structural elements of the buildings.

[7] The data compilation required a significant logistical effort because the RGNA data had to be extracted from assorted media, mostly magnetic tapes, located at each of the 15 GPS stations. We thus limited our data request to one 24-hour session per week for the period 1993 to June 2001, representing the entire period of observations at the time of our request. We received more than 95% of the data we requested, constituting more than 6000 station days of data or approximately 400 epochs per site (Table 2). Daily data from one station, Aguascalientes (INEG), have been archived since March 1998 at the Scripps GPS data archive and are also incorporated here. Data for site CULI for the year 1996 could not be retrieved from the magnetic media on which it was stored, representing the only significant data loss.

[8] Following conversion of the raw GPS data to RINEX format, we analyzed the GPS phase and code measurements using GIPSY analysis software, precise satellite orbits and clocks from the Jet Propulsion Laboratory (JPL), and a point-positioning strategy [*Zumberge et al.*, 1997] that we tailored for the Ashtech LM-XII3 data. Because the Ashtech LM-XII3 ceases tracking P code under antispoofing conditions, we instead employed the C/A code to generate improved estimates of time recorded by the relatively noisy receiver clocks. This proved extremely effective. Relative to a solution that employed only the phase measurements, use of the C/A code reduced the daily scatter in the site locations by factors of 5–10% in the north component, 40–50% in the east component, and 10–20% in the vertical component.

[9] Daily GPS station coordinates were first estimated in a no-fiducial reference frame [*Heflin et al.*, 1992] and were then transformed to ITRF2000 (http://lareg.ensg.ign.fr/ITRF/ITRF2000) using daily seven-parameter Helmert transformations supplied by JPL. Station velocities and antenna offsets were estimated via simultaneous linear regression of all three geocentric coordinate time series. The daily coordinates for a site are weighted using their variances and covariances. Daily intersite covariances are assigned values of zero, an outcome of our point-positioning data analysis strategy.

[10] One concern of ours was whether our use of the C/A code and phase measurements to solve for the RGNA station velocities might introduce a subtle systematic bias relative

Table 2. RGNA Site Velocities in ITRF2000[a]

Site	Time Span	Station Days	Velocities			Velocity Covariances					
			V_n	V_e	V_v	σ_{nn}	σ_{ee}	σ_{vv}	σ_{ne}	σ_{nv}	σ_{ev}
CAMP	5.825	275	−2.46	−6.33	0.57	0.99	1.65	4.37	−0.10	−0.30	0.54
CHET	8.208	363	−1.62	−5.66	−1.43	0.69	1.26	5.12	−0.06	−0.17	0.13
CHIH	8.299	401	−8.42	−10.17	1.01	0.70	3.30	1.91	0.37	−0.17	−0.26
CULI	8.164	338	−9.10	−9.24	1.39	0.62	0.92	2.68	−0.01	−0.01	−0.02
FMTY	8.208	401	−6.43	−10.49	2.36	0.67	1.04	3.45	0.20	−0.02	−0.05
HERM	8.351	405	−10.76	−11.83	5.02	0.64	0.94	2.45	0.25	−0.14	−0.13
INEG[b]	9.066	1303	−6.48	−10.74	−111.71	1.89	1.20	91.71	0.11	6.95	−2.27
LPAZ	8.118	457	19.50	−46.27	0.59	0.68	1.80	2.43	0.16	0.01	−0.24
MERI	8.186	400	−2.65	−5.64	−0.53	0.76	1.85	4.25	−0.37	0.12	−0.18
MEXI	8.353	350	12.23	−28.90	−1.30	0.92	1.43	1.32	0.18	−0.03	−0.17
OAXA	8.860	411	0.19	−6.98	0.84	1.00	2.11	3.80	0.46	0.15	0.20
TAMP	8.173	403	−5.86	−7.32	1.74	0.69	1.18	3.35	0.07	−0.15	−0.10
TOLU	8.353	390	−5.23	−4.09	−7.82	1.51	1.94	4.74	0.04	−0.77	−0.08
VILL	8.186	317	−3.41	−7.25	−2.77	1.05	1.85	6.44	0.14	−0.23	−0.72

[a]Velocities are given in millimeters per year and are specified relative to ITRF2000. Units of velocity covariances are $(\text{mm yr}^{-1})^2$. Velocities relative to the North American plate are given in Figures 3–5. The time span gives the length of the GPS time series in years. Station days specifies the number of days used to solve for the site velocity. Positive and negative vertical rates represent uplift and subsidence, respectively.

[b]Note that the vertical component of the velocity for INEG shown in Figure 4 is poorly fit by a linear model.

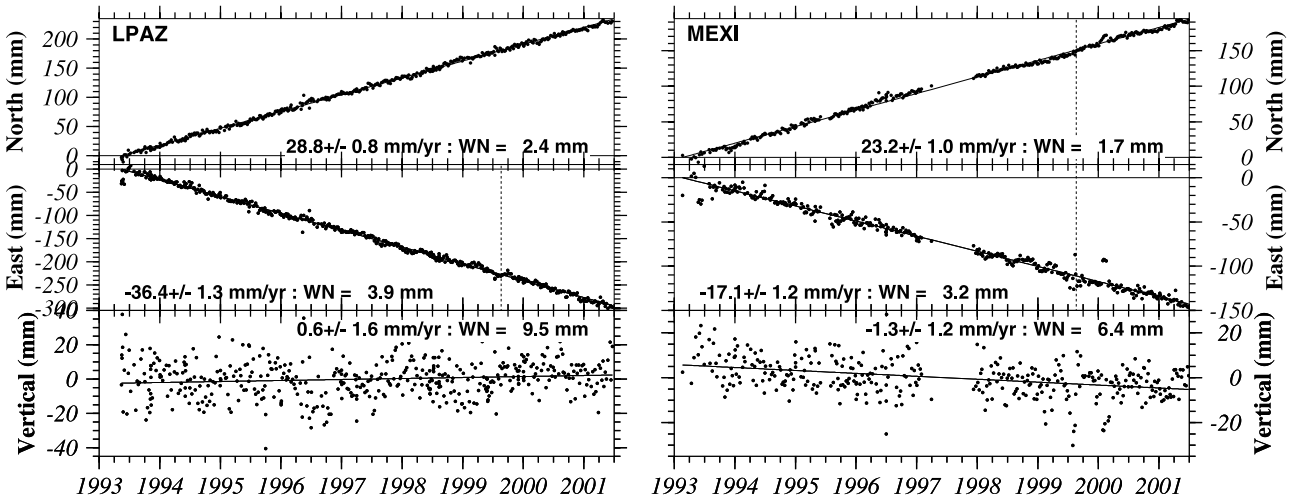

Figure 3. RGNA site displacements in north, east, and vertical directions referenced to motion of the North American (NA) plate (see text). Each point is determined from 24 hours of GPS data. Vertical dashed lines represent breaks in the GPS time series due to either antenna relocation or the GPS week roll-over (see text). Velocities and uncertainties represent the best fits to the residual displacements and incorporate uncertainties in both the observations and predicted motion of the North American plate. WN is the scatter (white noise) of the daily locations with respect to 30-day-average site locations. The dispersion of the numerous data about the linear fit is taken here to be the best estimator of the underlying uncertainties. Formal error bars for daily coordinates are thus omitted.

to GPS velocities that are estimated using phase and P code measurements. We tested for such a velocity bias by processing data from ten continuously operating P code receivers at assorted sites in the United States, first using the phase and P code measurements, and then using the phase and C/A code. For a given station, the horizontal velocities for the C/A and P code solutions never differed by more than 0.5 mm yr^{-1}, and more typically differed by no more than a few tenths of a millimeter per year. Mean differences in the north and east components for the P code and C/A code velocities for these ten sites are only 0.05 and 0.01 mm yr^{-1}, more than an order-of-magnitude smaller than any velocity that we interpret below. The mean difference in the vertical velocities, 1.3 mm yr^{-1}, is also significantly smaller than any vertical velocity that we interpret. We conclude that any systematic bias introduced into the GPS velocities via use of the C/A code instead of the P code is too small to affect any of the models or interpretations we describe below.

[11] We detected one unexplained artifact in the RGNA GPS data, a latitude-dependent ~35–50 mm westward displacement of the estimated site locations at the time of the GPS week rollover in August 1999. The artifact appears to result from a change in the firmware residing on all of the RGNA receivers on 20 August 1999, from its original LM-XII3 firmware to newer firmware written for Ashtech Z-XII receivers. Unfortunately, we were unable to locate anyone at Ashtech or INEGI with specific information about the now obsolete LM-XII3 firmware and its treatment of the raw data. That the change in site locations occurs only in the east component and decreases with increasing latitude strongly suggests that the two versions of the firmware treat time or a time-related observable differently.

[12] *McClusky et al.* [2001] describe a similar 20–50 mm artifact in Ashtech LM-XII data, and apply an empirical correction to their raw data. Given that such an empirical correction is inexact and could leave systematic biases of several millimeters in our site locations for times after 20 August 1999, we chose instead to solve for the 20 August 1999 offset in the east component when estimating the site velocities. This increases the uncertainty we estimate for the east component of the site velocities, but has no other effect.

[13] Prior to making any correction for the common mode errors that affect these and all of our other GPS time series (see below), the day-to-day scatter of the site coordinates relative to 30-day running averages in the coordinates were 3.5–4.3 mm in the north component, 4.5–6.4 mm in the east component, and 8.4–12 mm in the vertical component for the 14 RGNA sites. For comparison, the daily noise in the north, east, and vertical components for 160 other continuous GPS stations in North America (see below) averages 3.5, 5.5, and 9.9 mm, respectively. The data collected by the Ashtech LM-XII3 receivers thus yields coordinate time series of a quality comparable to those for continuous sites equipped with modern dual-frequency, P code receivers.

2.2. Other Data

[14] We also analyzed more than 280,000 station days of daily L1/L2/P code GPS observations from 160 sites on the North American plate (Figure 2) and 13 sites on the Pacific plate (Figure 2) with 2 years or more of continuous observations during the period 1 January 1993 through 1 March 2003. We selected these sites on the basis of their locations with respect to well-defined plate boundary structures, with no prejudice as to the type of monument on which the antenna was mounted. The North American plate sites include sites in southeastern California, Arizona, and New Mexico, which appear to be part of the stable interior

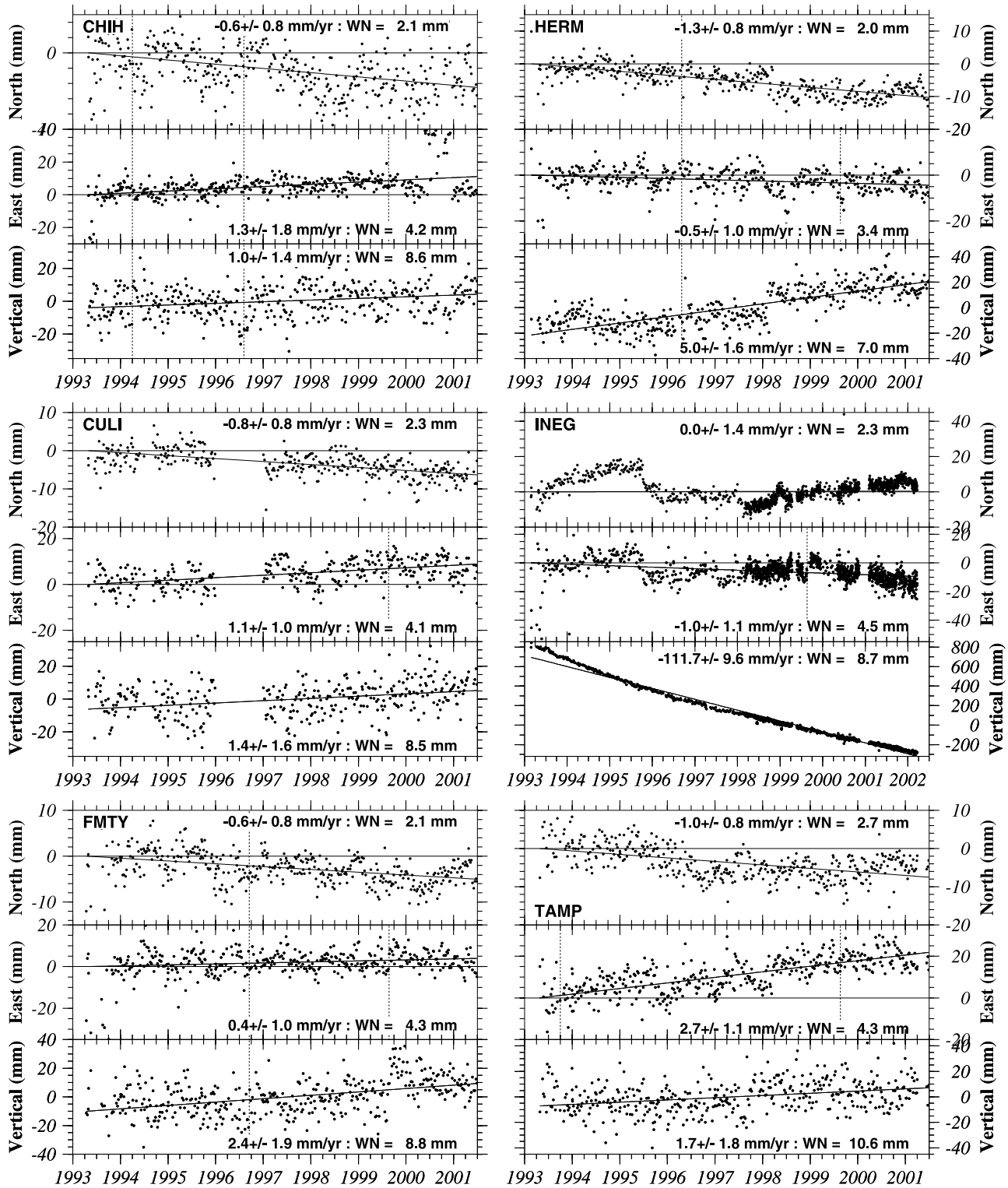

Figure 4. RGNA site displacements in north, east, and vertical directions referenced to motion of the North American plate. See caption to Figure 3.

of the North American plate [*Bennett et al.*, 1999] despite their locations west of the seismically active Rio Grande rift.

[15] Our 160-station North American plate solution excludes data from ten other sites that exhibit highly anomalous motion relative to stable North America. Three of these (BEA5, FMC1, and SHK1) were also excluded by *Gan and Prescott* [2001], who propose that monument instability is responsible for their anomalous motions. Anomalous motions at ARP3, AUS5, FMC2, FST1, HAMG, HDF1, and STL4, none considered by *Gan and Prescott* [2001], are also presumably caused by monument

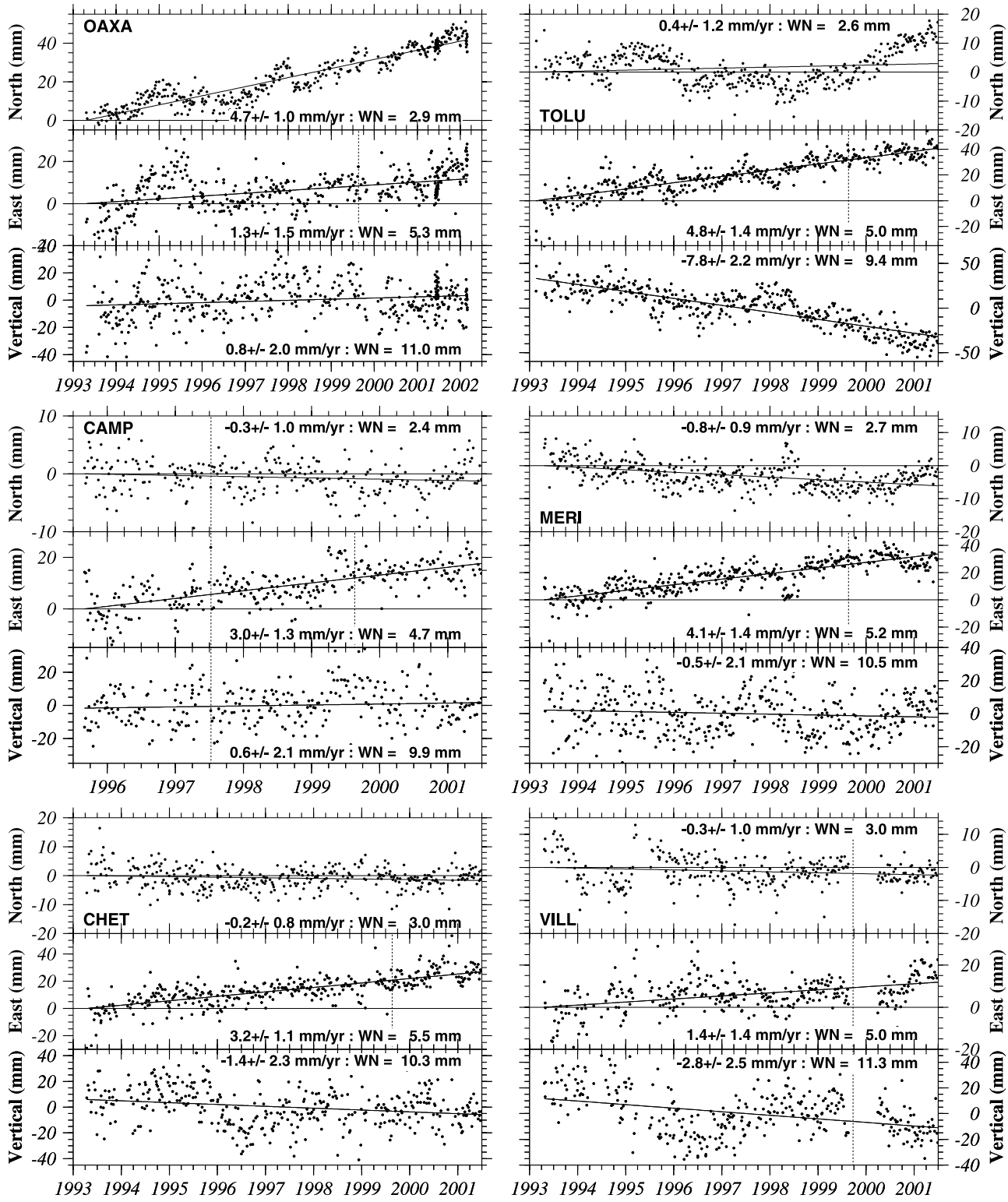

Figure 5. RGNA site displacements in north, east, and vertical directions referenced to motion of the North American plate. See caption to Figure 3.

instability, local geologic instability, or changes that affect propagation of the GPS satellite signals near the antenna.

2.3. Removal of Common Mode Station Noise

[16] All of the station velocities employed below are derived from time series of daily station coordinates that have first been corrected for the common mode components of noise that affect adjacent GPS sites. We estimate and remove the common mode noise using a new technique that allows for geographic variations in the character and amplitude of the common mode noise. Removal of the common mode noise and linear regression of the modified

time series employed below reduced the daily scatter to 2.3, 4.5, and 8.1 mm in the north, east, and vertical components, significantly smaller than for the unmodified time series (see above). Further details are given in Appendix A.

2.4. Site Velocities and Uncertainties

[17] The velocities and any unconstrained antenna offsets for all of the above sites relative to ITRF2000 were derived from inversions of individual site coordinate time series (Figures 3, 4, and 5), subject to a constant velocity constraint before and after any known or estimated antenna offsets. Table 2 lists the 14 RGNA station velocities. Uncertainties in the GPS velocities are determined using an error model that combines estimates of the white noise, flicker noise, and random monument walk present in a site's coordinate time series [*Mao et al.*, 1999]. We estimate the magnitudes of the white and flicker noise for each site directly from its coordinate time series, and further assume that all sites experience 2 mm/$\sqrt{\text{yr}}$ of random monument walk, in accord with an estimate reported by *Langbein and Johnson* [1997] for a site in southern California. The resulting standard errors in the north and east velocity components for the RGNA sites range from ± 0.8 to ± 1.4 mm yr^{-1}. Had we assumed a significantly slower rate of random monument walk, 1 mm/$\sqrt{\text{yr}}$, the velocity uncertainties would have been systematically smaller by 0.3–0.4 mm yr^{-1}. Given that the results described below are relatively insensitive to systematic changes in the velocity uncertainties, uncertainties in the magnitude of random monument walk do not constitute an important limiting factor in the analysis.

3. Results

[18] The North American and Pacific plates are the natural geological reference frames for the analysis below. We first derive angular velocity vectors (consisting of the pole coordinates and angular rotation rate) that best fit the motions of continuous GPS sites on these two plates and discuss the implications of the resulting velocity residuals for North American plate deformation. We then discuss the velocities of the 14 RGNA stations after removing plate motion predicted by the best fitting North American or Pacific plate angular velocity vectors. Uncertainties in the RGNA site velocities also include uncertainties propagated from the North American and Pacific plate angular velocity vectors. All velocity uncertainties quoted below are 1σ.

3.1. North American Plate GPS Velocity Field

[19] Using fitting functions described by *Ward* [1990], we inverted the 160 North American plate GPS velocities (Figure 6) to determine the angular velocity vector that minimizes the weighted, least squares fit (Table 3). Projection of the GPS station velocities onto small circles about the best fitting pole yields station rates that increase sinusoidally with angular distance from the best fitting pole, as expected (Figure 7). Similarly, the velocity components perpendicular to these small circles are zero within their

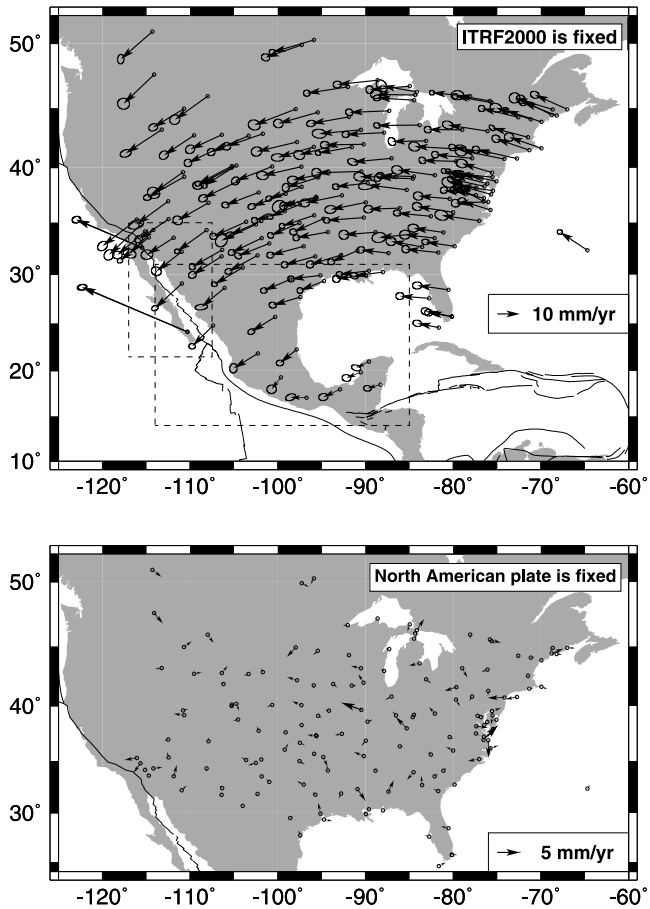

Figure 6. (top) Velocities of GPS sites relative to ITRF2000. Dashed rectangles show areas depicted in Figures 9 and 10. Velocities of some Pacific and North American plate sites included in Figure 1 are not shown but are used in the analysis. Uncertainty ellipses are 2-D, 1σ. All velocities are determined following correction of all GPS time series for common mode noise (see text). (bottom) Residual velocities of North American plate sites in the United States, Bermuda, and southern Canada. Frame of reference is the North American plate.

Table 3. Plate Angular Velocity Vectors[a]

			Angular Velocity			Covariances					
Plate	N	χ^2_ν	Latitude	Longitude	ω	σ_{xx}	σ_{yy}	σ_{zz}	σ_{xy}	σ_{xz}	σ_{yz}
NA	160	0.99	−5.95	−84.60	0.194	1.52	17.0	13.0	−0.01	0.07	−12.9
PA	13	1.07	−63.63	110.43	0.673	139.1	38.0	41.5	38.9	−17.9	−6.4

[a]Reference frame is ITRF2000. Positive angular rotation rates correspond to counterclockwise rotation about the pole. N is the number of GPS site velocities used to determine the best fitting angular velocity vector. χ^2_ν is the weighted least squares fit divided by the number of velocity components (2*N) − 3, the number of parameters adjusted to fit the data. Latitude and longitude are in °N and °E, respectively. The rotation rate ω has units of degrees per million years. Angular velocity covariances are Cartesian and have units of 10^{-10} rad^2/Myr^2. Abbreviations are NA, North American plate; PA, Pacific plate.

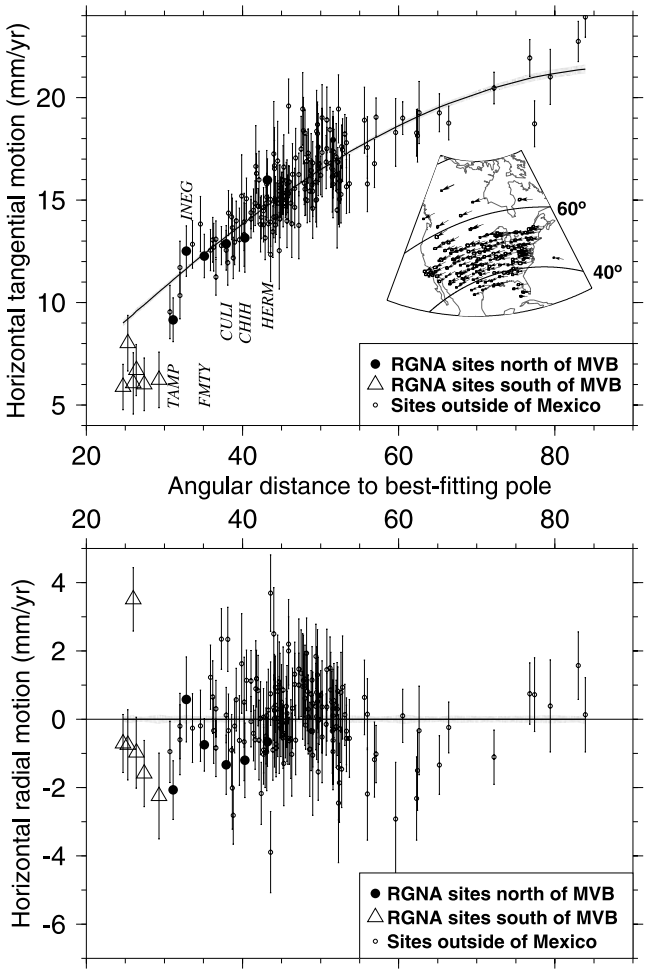

Figure 7. Velocity components for 160 North American plate and twelve RGNA sites relative to predictions (bold line) of the angular velocity vector that best fits the 160 North American plate GPS velocities. The geodetic reference frame is ITRF2000. (top) Tangential velocity components. These are determined by projecting the velocity at each site onto the small circle that passes through the site and is centered on the best fitting pole. All error bars are 1σ. (bottom) Radial horizontal velocity components. This component is perpendicular to the tangential component and should be zero since sites should move neither toward nor away from the pole of rotation. Stippled regions show 1σ uncertainties in the model predictions. MVB is Mexican Volcanic Belt.

uncertainties, as expected given that the stations should move neither toward nor away from the best fitting pole. Reduced chi-square for the best fitting angular velocity vector is 0.99, nearly equal to its expected value of 1.0. This suggests that the algorithm we employ to derive the velocity uncertainties is adequate.

[20] The best fitting angular velocity vector is strongly constrained by the 160 GPS site velocities and is highly robust with respect to the information contributed by the velocity of any single site. For example, at the location of site INEG in central Mexico, the uncertainties in the North American plate linear velocity predicted by the best fitting angular velocity vector are only ±0.13 mm yr^{-1} in both the north and east velocity components. The reference frame uncertainties are thus small in comparison to the ±1–2 mm yr^{-1} uncertainties in the RGNA station velocities.

[21] The formal data importance [*Minster et al.*, 1974], which quantifies the amount of information contributed by each site velocity to the best fitting angular velocity vector, indicates that the information that constrains the best fitting angular velocity vector is distributed relatively evenly amongst the 160 site velocities. None of the 160 velocities contributes more than 2.5% of the total information and only 20 contribute more than 1%. The sites with the highest importance tend to be sites located in geographically isolated locations (Bermuda, St. John's Island, Greenland) or with the longest record of observations. If we exclude the GPS velocity with the highest data importance and reinvert the remaining velocities, the modified North American plate angular velocity vector predicts motion in central Mexico that differs by less than 0.02 mm yr^{-1} from that predicted by the best fitting angular velocity vector. The predictions of the best fitting angular velocity vector are thus robust with respect to the information that is contributed by any single site velocity.

[22] The decrease in the magnitudes of the residual GPS rates with increasing observation time spans (Figure 8) supports our a priori expectation that the GPS rates averaged over the longest time spans should agree best with the predictions of a rigid plate model due to their improved averaging down of the short- and long-period departures from linear motion in their time series. The velocity residuals for the ten North American plate sites with time series longer than 9 years are smaller than 1.1 mm yr^{-1}

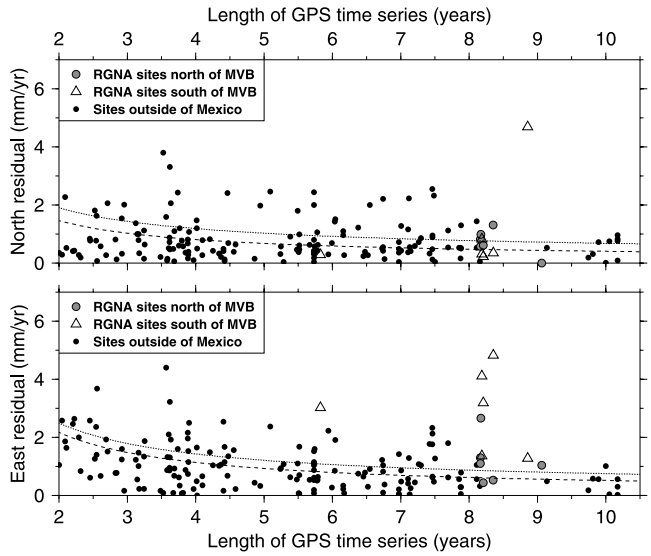

Figure 8. Residual velocity components for the 160 GPS sites used to estimate North American plate motion and the 12 RGNA sites. Residual motions are determined relative to velocities predicted by the best fitting North American plate angular velocity vector (Table 3). Curve shows average expected GPS site velocity uncertainties assuming average white and flicker noise contributions of 2.3 and 3.5 mm in the north component, 4.5 and 5.1 mm in the east component, and 1 mm $\sqrt{yr}^{-1}$ of random walk (see text).

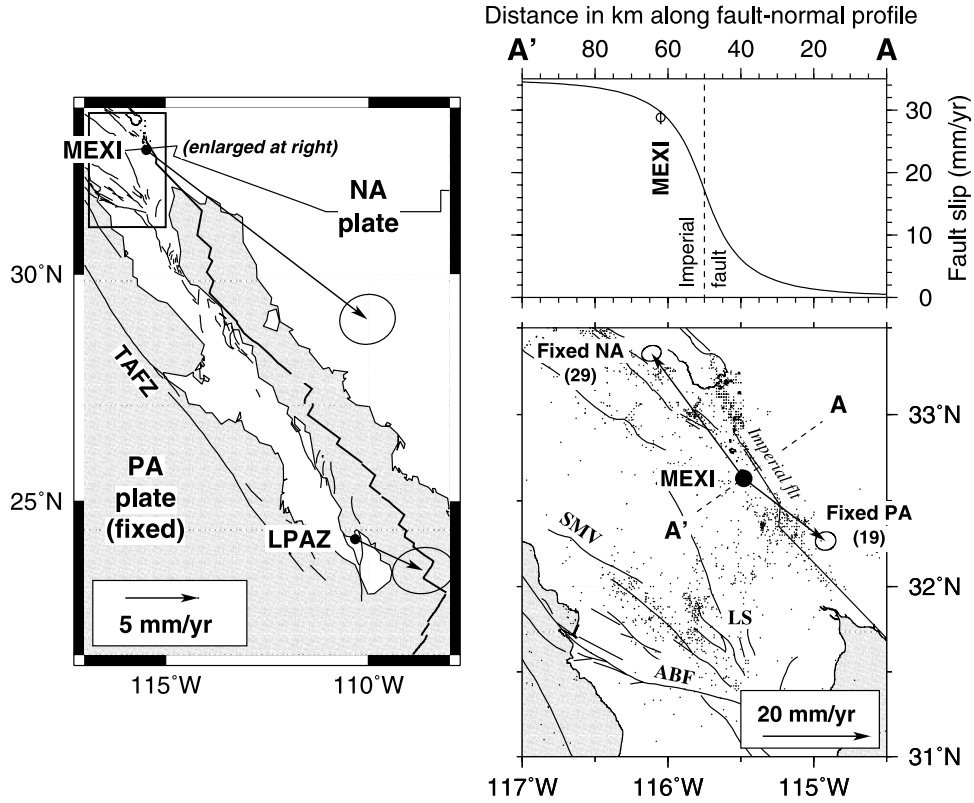

Figure 9. (left) Motions of LPAZ and MEXI relative to the Pacific plate. TAFZ, Tosco-Abreojos fault zone [*Spencer and Normark*, 1979]. (top right) Slip rates along profile A-A' predicted by a homogeneous elastic half-space model that assumes the Imperial fault is a 60-km-long vertical strike-slip fault that accumulates a 35 mm yr^{-1} slip deficit from the surface to 7.5 km depth. Predicted and observed slip rates are relative to the North American plate. (bottom right) Motion of MEXI relative to the Pacific (PA) and North American (NA) plates. Numbers in parentheses are rates in units of millimeters per year. Uncertainty ellipses are 2-D, 1σ. Dashed line shows locations of fault-normal profile A-A'. ABF, Agua Blanca fault; LS, Laguna Salada fault; SMV, San Miguel-Vallecitos fault.

(Figure 8), whereas residual velocities for sites with observations that span several years or less are more typically 1.5–3 mm yr^{-1}. That the stations with the longest time series have small residual velocities could also reflect the fact that most of those stations were installed by the International GPS Service (IGS) specifically for geodynamic studies and thus have relatively stable monumentation. Many of the stations with shorter time series were installed for nongeophysical purposes and are mounted on presumably less stable structures, including chimneys and steel towers.

[23] The scatter in the residual velocity field is comparable to that reported for previous studies. *Bennett et al.* [2002] report weighted root-mean-square (WRMS) misfits of 1.1 mm yr^{-1} to velocities of 59 sites in the plate interior. We inverted the velocities of 40 sites from our analysis that overlapped those of Bennett et al. and find WRMS misfits of 0.96 mm yr^{-1}. *Dixon et al.* [1996], *DeMets and Dixon* [1999], and *Kogan et al.* [2000] also report similar misfits to smaller sets of GPS velocities from the North American plate interior.

[24] The absence of obvious patterns in the residual velocity field (Figure 6) indicates that any internal deformation of the North American plate interior is smaller than the uncertainties in our site velocities. In particular, we do not observe any evidence for southward motion of the Mississippi embayment away from the plate interior, as reported by *Gan and Prescott* [2001] from an analysis of the velocities of 55 GPS stations in the central and eastern United States. Our velocity field includes more than 100 additional sites distributed over a significantly larger fraction of the North American plate, with many sites having time series longer than those employed by *Gan and Prescott* [2001]. We are thus unsure why we do not observe a similar pattern of residual velocities. Additional observations and analysis are clearly warranted, but are beyond the scope of this paper.

3.2. RGNA Sites in Baja California

3.2.1. LPAZ

[25] The GPS station in La Paz (LPAZ) lies more than 100 km west of the strike-slip faults in the Gulf of California that mark the Pacific-North America plate boundary (Figure 9). Its location west of nearly all of the plate boundary seismicity suggests that to first order, LPAZ should move with the Pacific plate. Contrary to this expectation, *Dixon et al.* [2000] report that the velocities for seven GPS sites in Baja California, including a velocity for LPAZ that was based on a preliminary version of our RGNA time series, exhibit a several millimeters per year boundary-

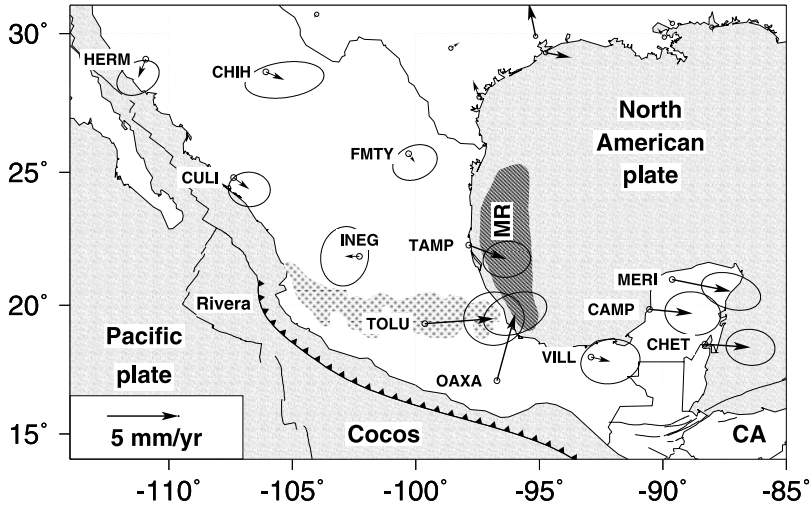

Figure 10. RGNA site velocities after removing motion of North American plate predicted by the best fitting North America-ITRF2000 angular velocity vector. Uncertainty ellipses are 2-D, 1σ. CA, Caribbean plate; MR, Mexican Ridges deformation belt. Stippled area shows extent of Mexican Volcanic Belt.

parallel slip deficit relative to Pacific plate motion. They interpret this as evidence that faults west of the Baja Peninsula still accommodate slow motion of the peninsula relative to the Pacific plate.

[26] We rotate the motion of LPAZ into a Pacific plate reference frame using an angular velocity vector (Table 3) that we derived from the velocities of 13 continuous GPS stations in the Pacific plate interior (Figure 2). Relative to ITRF2000, the best fitting Pacific plate angular velocity vector predicts motion of 53.5 ± 0.5 mm yr^{-1} toward N64.7°W ± 0.6° at a point in the Baja Peninsula (27.5°N, 113.0°W). This differs little from motion predicted by the Pacific plate angular velocity vector of *Dixon et al.* [2000] (53.4 ± 1.4 mm yr^{-1} toward N65.7°W ± 1.6°), even though we employ more GPS velocities (13 versus 5), longer GPS time series, and a more recent geodetic reference frame (ITRF2000 versus ITRF1996).

[27] Our updated GPS time series at LPAZ is based on many more station days than were used to derive the preliminary time series presented by *Dixon et al.* [2000] and hence allows for a stronger test of the hypothesis that the Baja Peninsula is detached from the Pacific plate. Relative to the Pacific plate, LPAZ moves 5.1 ± 1.3 mm yr^{-1} toward S65°E ± 11° (Figure 9), subparallel to the strike-slip faults in the southern Gulf of California. Our result thus corroborates the boundary-parallel slip deficit reported by *Dixon et al.* [2000]. Following *Dixon et al.* [2000], we interpret this as evidence that at least part of the Baja Peninsula is presently detached from the Pacific plate, possibly along offshore faults such as the Tosco-Abreojos fault zone.

3.2.2. MEXI

[28] The GPS station in Mexicali is located 12 km southwest of the Imperial fault (Figure 9), which accommodates right-lateral strike-slip motion between the Pacific and North American plates. Numerous earthquakes occur along faults to the west and south of Mexicali, indicating that MEXI moves relative to the Pacific plate. Similarly, earthquakes along the Imperial fault just northeast of MEXI indicate that it also moves relative to the North American plate. We thus expect the motion at MEXI to be intermediate between Pacific and North American plate motion, with a strong contribution from elastic strain due to frictional locking of the Imperial fault. Below, we discuss its motion relative to both plates.

[29] Relative to the North American plate, MEXI moves 28.8 ± 1.0 mm yr^{-1} toward N36°W ± 2°, parallel within uncertainties to the adjacent Imperial fault, which strikes N38°W ± 1° (Figure 9, bottom right). Assuming that the Imperial fault is well approximated as a vertical, strike-slip fault that accrues an elastic slip deficit of 35 ± 2 mm yr^{-1} above depths of 7.5 km, as proposed by *Bennett et al.* [1996], a homogeneous elastic half-space model (Figure 9, top right) predicts that MEXI should accrue a fault-parallel slip deficit of 29.8 mm yr^{-1} relative to stable lithosphere far northeast of the Imperial fault (e.g., the North American plate). The predicted and observed rates thus differ by only 1 mm yr^{-1}, well within their combined uncertainties. The GPS velocity at MEXI is thus consistent with a simple preexisting model for slip along this fault. An alternative model for slip along the Imperial fault that incorporates near-surface fault creep and elastically stored slip at depths greater than 9 km [*Genrich et al.*, 1997] could be tested by combining the velocity at MEXI with additional near-fault observations.

[30] We thus find that in a fixed North American plate reference frame, the observed and predicted rates at MEXI agree well, and MEXI's direction of motion is parallel within uncertainties to the strike of the Imperial fault. This implies that any permanent deformation of the North American plate (northeast of the Imperial fault) must be slower than the 1–2 mm yr^{-1} uncertainties in the velocity for MEXI. This conclusion agrees with evidence reported by *Bennett et al.* [1999, 2002] that GPS sites in southeastern California move with the North American plate interior.

[31] Relative to the Pacific plate, MEXI moves 19 ± 1 mm yr^{-1} toward S53°E ± 4° (Figure 9), 15° oblique to the trend of the Imperial fault and much faster than the

5 mm yr^{-1} rate predicted by an elastic half-space model constructed for a Pacific plate reference frame. The fact that neither the observed direction nor rate agree with those predicted by a model that assumes Pacific plate lithosphere extends to the southwestern edge of the Imperial fault corroborates geodetic, geologic, and seismologic evidence for significant slip along faults south and west of the Imperial fault, including the Laguna Salada, San Miguel-Vallecitos, and Agua Blanca faults [*Bennett et al.*, 1996].

3.3. RGNA Sites in Mainland Mexico

[32] Figure 10 shows the first ever large-scale view of the present velocity field of Mexico with North American plate motion removed. Our goal below is to present the simplest interpretation of the velocity field that is consistent with both the data and what is known about the present neotectonics of Mexico. We focus primarily on patterns of motion that are exhibited by multiple, adjacent sites, which we believe are more likely to be robust than the motion of any individual site.

[33] Much of northern Mexico is affiliated morphologically and tectonically with the southern Basin and Range province of the United States [*Suter and Contreras*, 2002]. Given that GPS sites within the southern Basin and Range province of the United States move with the North American plate interior within their 1–2 mm yr^{-1} uncertainties [*Bennett et al.*, 1999], it seems equally likely that the RGNA sites located north of the Mexican Volcanic Belt also move as part of the North American plate interior. We test this hypothesis first, after which we extend our analysis to sites within and south of the Mexican Volcanic Belt.

3.3.1. Sites North of the Mexican Volcanic Belt

[34] The residual velocities of four of the six RGNA stations north of the Mexican Volcanic Belt (CHIH, CULI, FMTY, INEG) are zero within their estimated 2-D, 1σ uncertainties (Figure 10), and the motion of station HERM exceeds its estimated uncertainty by only tenths of a millimeter per year. Given that these five sites span most of Mexico north of the volcanic belt, their insignificant motions relative to North America imply that the stable North American plate interior extends at least as far south as the Mexican Volcanic Belt. Further below, we discuss possible reasons for the ESE directed motion of site TAMP relative to North America.

[35] We use the *Stein and Gordon* [1984] test for an additional plate to determine whether the velocities of the six sites north of the volcanic belt (CHIH, CULI, FMTY, HERM, INEG, TAMP) are consistent with North American plate motion. Simultaneous inversion of these six velocities and the 160 North American plate site velocities to find their best fitting angular velocity vector yields a RMS misfit of $\chi^2 = 327.1$, whereas separate inversions of the six RGNA station velocities and the 160 North American plate site velocities to solve for their respective best fitting angular velocity vectors yields a combined RMS misfit of $\chi^2 = 320.7$. The difference in the least squares fit of the two models, $\Delta\chi^2 = 6.4$, is significant at only the 90% confidence level. If we remove the velocity for site TAMP, which is located directly onshore from an extensive offshore gravity slide (discussed below), and repeat the above inversions, the difference between the RMS fits of the separate and combined data sets decreases to $\Delta\chi^2 = 3.8$, significant at only the 71% confidence level.

[36] On the basis of these results, we conclude that the RGNA station velocities for sites located north of the Mexican Volcanic Belt are consistent with the hypothesis that the stable plate interior extends southward to at least the northern limit of the Mexican Volcanic Belt.

3.3.2. Implications for Motion Across the Mexican Basin and Range

[37] The velocities of stations CULI and HERM, which are located west of nearly all of the Mexican Basin and Range structures (Figure 2), provide useful limits on the present rate of extension across this region. Within the 95% error ellipses of the residual velocities at CULI and HERM, the maximum rates of west to southwest directed motion at these two sites are 1.5 and 3.0 mm yr^{-1}, respectively. Similarly, within the 95% confidence ellipse for CHIH, near the geographic midpoint of the Mexican Basin and Range, motion of this site toward the west or southwest must be slower than 3.0 mm yr^{-1}. The lower limit for any component of west or southwest directed extension is zero at all three sites. The velocities at all three sites are thus consistent with no extension across the Mexican Basin and Range and suggest an upper 95% limit of ~1–3 mm yr^{-1} for west or southwest directed extension. Deformation within this region evidenced by large historic earthquakes [*Doser and Rodríguez*, 1993; *Suter*, 2001; *Suter and Contreras*, 2002] and faults that offset Quaternary features [*Henry and Aranda-Gomez*, 1992] must thus result from thin-skinned extension not recorded by CULI and HERM or must be slower than the ~1–3 mm yr^{-1} limit suggested by the velocities at CULI and HERM.

3.3.3. TAMP and the Mexican Ridges Deformation Belt

[38] Site TAMP, located in Tampico on the gulf coast of Mexico, moves 2.8 ± 1.0 mm yr^{-1} toward S70°E ± 18° (Figure 10) in a North America fixed frame. Assuming that the ESE directed motion of this site is not an artifact of building instability, there are at least two possible explanations for its motion.

[39] One possibility is that the seaward motion of TAMP is related to active deformation within the Mexican Ridges deformation belt in the western Gulf of Mexico. The Mexican Ridges fold belt is a 50- to 70-km-wide zone of prominent, offshore sediment folds that parallel the gulf coast of Mexico for more than 500 km [*Bryant et al.*, 1968]. Near Tampico, the axes of these active folds trend in a north-northwest direction. Marine seismic lines 100 km southeast of Tampico show that these folded sediments are decoupled from lower, undeformed sediments along a decollement within a thick shale section [*Buffler et al.*, 1979]. *Pew* [1982] summarizes evidence that the folding results from east directed gravity sliding along this decollement, possibly representing the largest active submarine landslide in the world.

[40] In light of the ESE directed motion at TAMP and eastward gravity sliding of the offshore sediments, TAMP may be moving downslope behind the trailing edge of the offshore gravity slide. Active growth faults representing the head scarps of the decollement at the base of the gravity slide are located offshore [*Buffler et al.*, 1979], indicating that TAMP cannot be moving at the full downslope rate. If

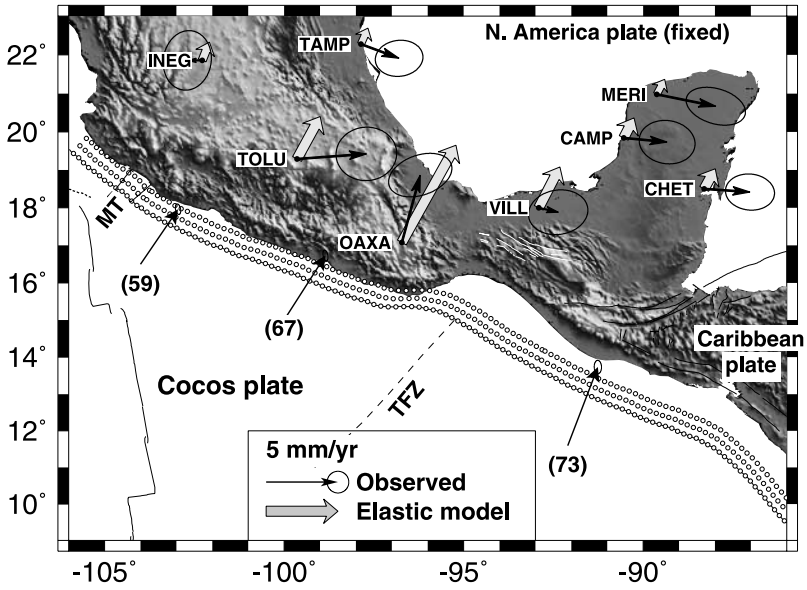

Figure 11. Observed GPS velocities at sites in southern Mexico compared to velocities predicted from elastic half-space modeling of the Rivera-North America, Cocos-North America, and Cocos-Caribbean subduction interfaces. All velocities are relative to the North American plate. Offshore velocity arrows are predicted plate convergence velocities (see text), with rates in millimeters per year specified by the numbers within the parentheses. Dashed line designates location of the Tehuantepec fracture zone (TFZ). MT designates the Manzanillo trough, an offshore graben assumed here to separate subducting Rivera plate lithosphere to the northwest from subducting Cocos plate lithosphere to the southeast. The three subduction interfaces are divided into subfaults, each of which is assumed to accumulate strain in the predicted plate convergence direction at the full, geographically varying plate rate (see text). Circles depict the upper midpoint of each subfault. Faults that accommodate 20 mm yr^{-1} of sinistral slip between the Caribbean and North American plates contribute negligible additional motion (<0.1 mm yr^{-1}) at these sites. Velocity error ellipses are 2-D, 1σ.

the offshore decollement is locked by friction, motion at TAMP may represent an elastic response to that locking. Borehole strain measurements in the Tampico region yield a mean direction of S69°E ± 6° for the regional minimum horizontal stress [*Suter*, 1987], possibly offering additional evidence that the east directed offshore slumping influences both the regional stress and strain.

[41] A second possibility, suggested by one of our reviewers, is that TAMP moves with sites CAMP, CHET, and MERI, which are located several hundred km to the east in the Yucatan Peninsula and also move toward the ESE at similar rates (Figure 10). Assuming this is correct, it is unclear why VILL, which lies midway between TAMP and the Yucatan Peninsula sites, does not also move at the same eastward rate. Measurements at additional GPS sites onshore from the Mexican Ridges deformation belt and elsewhere along the gulf coast of Mexico would provide a strong basis for testing both of these hypotheses.

3.3.4. INEG: Subsidence From Groundwater Withdrawal

[42] Located in a graben within the southern Mexican Basin and Range, the RGNA site in the city of Aguascalientes (INEG) is subsiding more than 100 mm/yr (Figure 4). With only 30 cm of annual precipitation, the majority of the agriculture in the vicinity of the city relies on irrigation. Substantial withdrawal of groundwater from the aquifers underlying the city is presumably responsible for the rapid subsidence, totaling more than 1 m since 1993. An inspection of the linear fit to the vertical time series clearly shows that the rate of subsidence has decreased since 1993. This agrees qualitatively with the predictions of a model in which water is withdrawn at a uniform rate from a half-space; such a model predicts that the rate of surface subsidence decays logarithmically as the decreasing fluid pressure allows for compaction of the water-bearing sediments [*Wang*, 2000]. Despite the rapid subsidence at this site, the horizontal site motion agrees surprisingly well with that predicted by the North American plate angular velocity vector (Figure 10).

3.4. Sites Within and South of the Volcanic Belt

[43] Five of the six GPS stations within or south of the volcanic belt move significantly relative to the North American plate (Figure 10). The nonzero residual velocities of OAXA and TOLU are not surprising given that motion at OAXA is significantly influenced by elastic strain accumulation along the Cocos-North America subduction interface (discussed below) and TOLU is located within the Mexican Volcanic Belt. The eastward translations of the four GPS stations in and near the Yucatan Peninsula (CAMP, CHET, MERI, and VILL) are unexpected and suggest modifications to existing models of Mexican neotectonics.

3.4.1. OAXA: Elastic Strain Accumulation

[44] The GPS station at OAXA moves 4.9 ± 1.2 mm yr^{-1} toward N15°E ± 16°, roughly perpendicular to the nearby Middle America trench (Figure 10). Trench-normal strain accumulation is commonly observed at GPS sites close to

subduction zones, thereby suggesting an obvious explanation for the northeast directed motion at OAXA.

[45] We tested the hypothesis that motion at OAXA and possibly other RGNA sites results principally from strain accumulating along the upper locked regions of the Middle American subduction zone by constructing a homogeneous elastic half-space within which we embedded the Middle America subduction interface. We approximated the subduction interface as a mesh of rectangular subfaults (Figure 11) that extend from the northwestern terminus of the subduction interface, where Rivera plate subduction occurs, to the southeastern terminus of the Cocos-Caribbean subduction interface. Each subfault extends 20 km along the local strike of the trench, 30 km downdip, and accumulates a downdip slip deficit at a rate equal to the full plate convergence rate predicted at the subfault location. Rivera-North America plate convergence velocities are predicted using an angular velocity vector from *DeMets and Wilson* [1997]. Cocos-North American plate and Cocos-Caribbean plate motions are predicted using angular velocity vectors from *DeMets* [2001].

[46] We assume that the locked portion of the subduction interface extends to an average depth of 25 km, as appears to be the case for at least some areas of the Middle America subduction zone [*Suárez and Sánchez*, 1996; *Hutton et al.*, 2001]. We assign a dip of 15° to all subfaults and note that the elastic model predictions for sites farther than 100 km from the trench are relatively insensitive to a range (10°–20°) of plausible assumed dips for the subduction interface. Our elastic model employs equations from *Okada* [1985] and produces as its output the predicted velocities of sites along the upper surface of the elastic half-space.

[47] Relative to the North American plate, the elastic velocity predicted at OAXA is 8 mm yr^{-1} toward the northeast, faster than and in a direction close to the observed residual velocity for OAXA (Figure 11). Given our assumption that the subduction interface is fully locked, the elastic slip deficits predicted by our model represent an upper bound on the possible influence of elastic strain. The faster predicted rate could indicate that Cocos-North America convergence is accommodated partly by creep along the subduction interface. This interpretation is consistent with estimates of seismic coupling along the Middle America trench, which suggest that earthquakes typically accommodate half or less of the predicted plate convergence along much of the subduction zone [*Pacheco et al.*, 1993]. Alternatively, upper crustal shortening may occur between OAXA and the trench, thereby accounting for the observed difference, or our elastic model may be too simplistic.

[48] The elastic velocities predicted for RGNA sites farther inboard are 0.5–3 mm yr^{-1} toward the northeast (Figure 11). The failure of the elastic model to fit any of the other residual GPS velocities may result from some of the same factors (partial coupling of the Middle America seismogenic interface or permanent deformation of the upper crust) that are discussed above.

3.4.2. TOLU: Subsidence From Groundwater Withdrawal

[49] The GPS station in the city of Toluca is located in a graben within the Mexican Volcanic Belt, 20 km north-northeast of Nevado de Toluca, a 4690-m-high active stratovolcano. The city is built on volcanic and lacustrine deposits that are actively pumped for irrigation and industrial purposes. Both the vertical and horizontal motions of this station differ significantly from zero, with vertical subsidence of 8 ± 2 mm yr^{-1} and horizontal motion of 4.8 ± 1.4 mm yr^{-1} toward N86°E ± 15°.

[50] The most obvious explanation for the observed subsidence at TOLU is groundwater withdrawal, although we cannot exclude the possibility that some or all of the subsidence is related to faulting or the nearby volcano. Eastward motion of this site has at least three possible explanations, including possible instability of the four-story building that hosts the GPS antenna, deformation related to the nearby stratovolcano, or possible left-lateral, transtensional motion across the Mexican Volcanic Belt. Additional velocities from a denser network in this area are needed to distinguish between these possible explanations.

3.4.3. CAMP, CHET, MERI, and VILL: Evidence for a Yucatan Block?

[51] The most unexpected result of our analysis is the eastward motion of CAMP, CHET, MERI, and VILL, all located on or near the Yucatan Peninsula (Figure 10). The respective speeds of these sites, 3.0 ± 1.3, 3.2 ± 1.1, 4.2 ± 1.4, and 1.4 ± 1.3 mm yr^{-1} are remarkably consistent within their uncertainties, as are their directions of motion. We tested whether the eastward motions of these four sites relative to the North American plate are statistically significant by using the *Stein and Gordon* [1984] test for an additional plate. Simultaneous inversion of these four RGNA velocities and 160 North American plate site velocities to find the RMS misfit (χ^2) for a single, best fitting angular velocity vector gives $\chi^2 = 335.6$. In contrast, inverting the two sets of velocities separately to determine best fitting angular velocity vectors and RMS misfits for each gives a combined least squares misfit of $\chi^2 = 314.7$. The likelihood that the difference in the RMS fits of the two models, $\Delta\chi^2 = 20.9$, results solely from random errors in the site velocities is only $9 * 10^{-5}$. The two sets of velocities are thus inconsistent with each other at a high confidence level (99.99%).

[52] It seems unlikely that problems with the raw GPS data, our analysis techniques, or spatially correlated noise in the GPS time series could be responsible for the apparent eastward motions of CAMP, CHET, MERI, and VILL relative to the North American plate. If this were the case, we would expect to observe similar biases in the GPS velocities for the other nine RGNA sites. We do not observe this: the velocities of five of the six RGNA stations north of the Mexican Volcanic Belt and the motion at OAXA all conform to our a priori expectations for their behavior at the sub-2 mm yr^{-1} level. In addition, our comparison of velocities we derived from C/A code and P code observations from modern P code receivers (described above), and our comparisons of the noise characteristics of the coordinate time series for the RGNA sites and other sites with modern P code GPS receivers reveal no evidence of systematic biases or excessive noise in the RGNA GPS data. We also note that CAMP, CHET, MERI, and VILL are located more than 100 km from each other and are thus unlikely to have highly correlated sources of local geologic and monument noise. Finally, the GPS time series for these four sites are well-behaved, linear, and span long enough periods (8.2 yrs to 5.8 yrs) to average down long-period noise that contaminates

their velocities. For these reasons, we are confident in both the accuracy and precision of the velocities of the four sites in and near the Yucatan Peninsula.

[53] Given that the eastward velocities of these sites are unlikely to be an artifact of the raw data or processing techniques, we examined whether elastic strain or possibly a transient viscoelastic response to a large earthquake along either the Middle American subduction interface or Motagua fault could be responsible. These also appear to be unlikely explanations. Our elastic half-space model (described above) predicts maximum elastic velocities (Figure 11) that are slower than and in a significantly different direction than the residual velocities at CAMP, CHET, MERI, and VILL. Adding the Motagua fault, which accommodates 20 mm yr^{-1} of left-lateral slip [*DeMets et al.*, 2000] and has been accumulating strain since its last major rupture in 1976, only changes the predicted elastic slip deficits by 0.1 mm yr^{-1}.

[54] We predicted the viscoelastic response to earthquakes along the Middle America trench using a three-dimensional finite element model with properties identical to those described by *Masterlark et al.* [2001]. The most recent, largest magnitude rupture of the Middle America subduction interface near the Yucatan Peninsula occurred on 29 November 1978, when a M_s = 7.8 shallow thrust earthquake accommodated ~1.2 m of downdip slip along an 85-km-long segment of the subduction interface offshore from Oaxaca [*Chael and Stewart*, 1982].

[55] Assuming a uniform viscosity of 1×10^{19} Pa s for the upper mantle and lower crust [*Wang et al.*, 2001], the viscoelastic response for the period 1993 to June 2001, spanning the RGNA GPS measurements, ranges from 1 mm yr^{-1} at VILL to only 0.1 mm yr^{-1} at CAMP, CHET, and MERI, much slower than observed. Moreover, the predicted directions point toward the west-southwest, nearly opposite the observed eastward motions of these sites. Using higher or lower viscosities for the lower crust and upper mantle would not significantly alter the predicted directions. Any viscoelastic response to the 1976 Motagua fault M_s = 7.5 earthquake, which was smaller than the 1978 Oaxaca earthquake and was centered more than 300 km from the closest of the four sites (VILL), is unlikely to be measurable at the distant Yucatan Peninsula sites.

[56] In light of the apparent failure of the above explanations for the eastward motions of the Yucatan Peninsula sites, we explored the hypothesis that the Yucatan Peninsula could be part of a larger crustal block that moves relative to the North American plate. If this is true, some deformation, possibly distributed across a wide zone, should occur around this block. The evidence for any such deformation in the Gulf of Mexico or Caribbean Sea is weak. A region of distributed shallow earthquakes in the Bay of Campeche (Figure 1), west of the Yucatan Peninsula, may record deformation along one side of the proposed Yucatan block. No focal mechanisms for these small-magnitude earthquakes are available. East of the peninsula, marine seismic reflection data compiled from the Yucatan basin do not reveal any folding or faulting of young sediments [*Rosencrantz*, 1990] that might accompany eastward translation of the peninsula. Moreover, the Yucatan basin and areas of the Gulf of Mexico north of the peninsula are nearly aseismic (Figure 1).

[57] Relating deformation onshore to possible motion of the Yucatan block is equally difficult. Deformation in the Isthmus of Tehuantepec and within lithosphere located southwest of the Yucatan Peninsula may be related to the poorly understood transition from Caribbean plate lithosphere to North American plate lithosphere [*Guzmán-Speziale et al.*, 1989]. In addition, deformation in this region may be influenced by ongoing subduction of the Tehuantepec ridge, an oceanic fracture zone that marks a transition from shallow subduction northwest of the fracture zone to steep subduction to the southeast [*Burbach et al.*, 1984; *Ponce et al.*, 1992].

4. Discussion and Conclusions

[58] Our interpretation of the present velocity field of Mexico is clearly nonunique and will certainly be revised by ourselves and other authors once additional continuous GPS sites in Mexico yield well constrained velocities. The results however present fertile grounds for future studies and debate, particularly in regard to the implications for any slip across the Mexican Volcanic Belt and for the unexpected eastward motions of sites in the Yucatan Peninsula.

[59] The new velocity field places only broad constraints on the amount of present-day slip that might occur across the Mexican Volcanic Belt. One end-member interpretation of our results, based on the velocities of TOLU and the three Yucatan Peninsula stations is that sinistral slip as rapid as 3–4 mm yr^{-1} occurs across the volcanic belt. The other extreme interpretation, based on the velocities of stations OAXA and VILL, is that no motion occurs across the volcanic belt. The latter interpretation, which implies that undeformed North American plate lithosphere extends far into southern Mexico, is consistent with an independent, structurally based estimate of 0.2 mm yr^{-1} for the rate of integrated slip across faults in the volcanic belt [*Suter et al.*, 2001].

[60] The lack of a compelling explanation for the eastward motions of the RGNA sites in the Yucatan Peninsula is clearly unsatisfying. At present, we prefer the least astonishing explanation, namely, that the Yucatan Peninsula moves slowly eastward as a coherent or nearly coherent block. We note however the geologic and seismologic evidence to corroborate this hypothesis are weak. Although it is also possible that thin-skinned detachment of the upper crust in the Yucatan Peninsula allows for coherent, east directed slip at CAMP, CHET, and MERI, the mechanism for achieving coherent, thin-skinned translation of the upper crust over such a large area is unclear and is thus unappealing. Another possibility is that the eastward motions are a regional artifact of long-term instabilities in the geodetic reference frame we employ. We consider this unlikely, but cannot exclude it without additional years of measurements.

[61] Assuming that a Yucatan block exists, existing observations limit its geographic extent. Station VILL moves ~2 mm yr^{-1} more slowly to the east than do the three sites in the Yucatan Peninsula (CAMP, CHET, and MERI), possibly indicating the approximate western limit to the Yucatan block. The good agreement between the observed direction of station OAXA and that predicted by our elastic model (Figure 11), coupled with structural evidence that the bulk Neogene motion across the Mexican

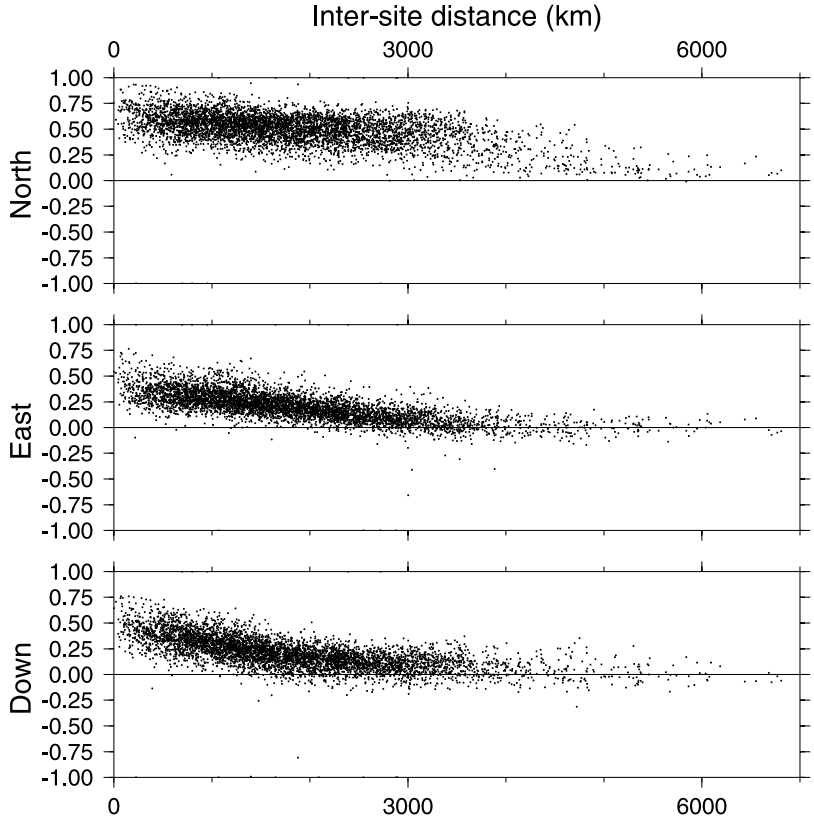

Figure 12. Correlation coefficients between residual values of continuous GPS coordinate time series for sites in North America and Mexico as a function of distance between sites. Daily residual values for a given site are determined from linear regression of the daily estimates of a site's coordinates. Each correlation coefficient is determined from cross correlation of the daily residual values for two GPS site time series. Site locations are shown in Figure 2.

Volcanic Belt consists of NNW-SSE oriented extension of 0.2 ± 0.05 mm yr^{-1} [*Suter et al.*, 2001] both reinforce the idea that the western limit to the Yucatan block lies well south of the Mexican Volcanic Belt.

[62] If there is an eastward translating Yucatan block, we can only speculate about what forces drive its motion. The absolute motion of the North American plate in the center of the Yucatan Peninsula, 30 mm yr^{-1} toward S67°W [*Gripp and Gordon*, 1990], carries the Yucatan Peninsula toward the shallowly subducting Cocos slab and toward continental lithosphere that is trapped in the zone of distributed deformation between the Caribbean and North American plates. Both impede the southwestward absolute motion of the Yucatan Peninsula as part of a rigid North American plate and hence may force slow eastward motion of the Yucatan Peninsula in a North American plate reference frame.

Appendix A: Removal of Common Mode Station Noise

[63] Daily and longer-period departures from linear motion at a given GPS site are caused by a variety of random and time-correlated sources of noise, some of which are site-specific and others of which are regionally correlated. Errors in the satellite orbits, water loading from the atmosphere and hydrosphere [*Van Dam et al.*, 2001], and uncertainties in daily and long-term geodetic reference frame definition can all cause regionally correlated errors in estimates of daily GPS site coordinates. In contrast, site specific errors can result from unrepaired slips in GPS phase counts, changes in the electrical or multipath environment of a GPS antenna, and random and/or systematic walk of a GPS monument.

[64] We examined the relative contributions of site-specific and common mode noise in our data by comparing the daily residual value of the latitudinal (north), longitudinal (east), and vertical component for each GPS site after removing the best linear fit to that site's point-positioned coordinate time series. A cross correlation of the residual time series for the numerous sites employed in our analysis clearly illustrates that a substantial fraction of the noise is correlated between sites (Figure 12). For example, sites separated by less than $\sim$1000 km have correlation coefficients as high as 0.95 for the north residual components. A gradual decrease to zero in the intersite correlations for sites separated by more than 6000 km suggests there is a distance-dependent loss of coherence in the processes responsible for the correlated noise. Correlation coefficients for the east and vertical components exhibit similar distance-dependent behavior, but have lower overall correlation coefficients.

[65] Prior authors have applied two techniques to remove common mode noise from regional-scale GPS networks.

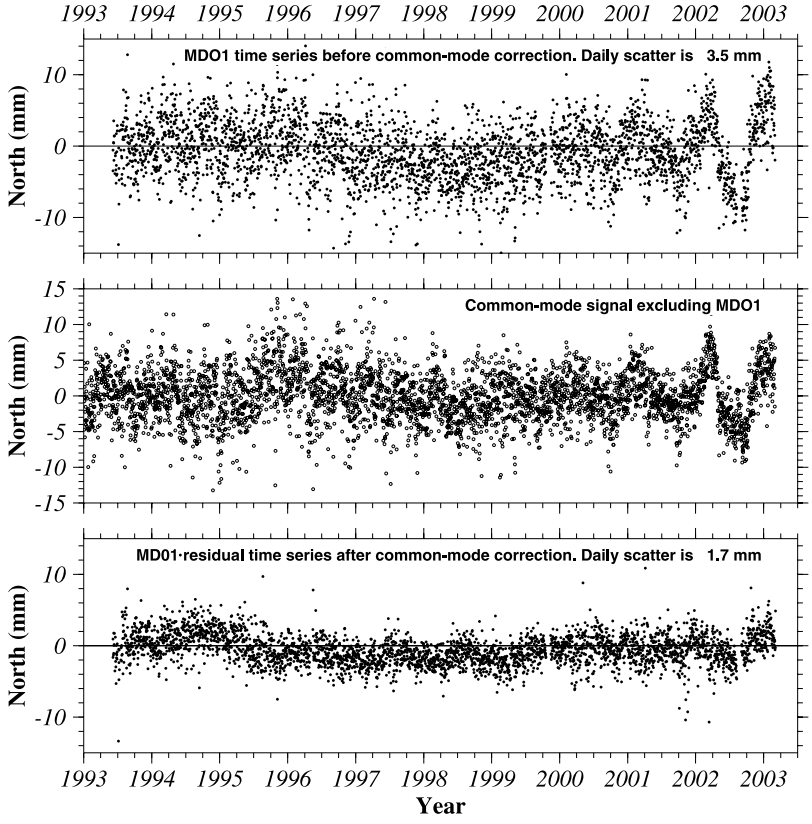

Figure 13. Effect of common mode correction to north component of the GPS time series for site MDO1 at the Macdonald Observatory, Texas. (top) Motion of MDO1 with its best fitting slope removed and prior to any correction for the common mode daily noise. (middle) A weighted average of the daily noise estimated from the daily linear residual north components for continuous GPS sites within 2000 km of MD01, excluding MDO1 and any sites with time series shorter than 2.0 years. (bottom) MDO1 time series reduced by its new best fitting slope after correction for the common mode noise shown in Figure 13 (middle).

Wdowinski et al. [1997] employ stacking of the residual errors from linearly detrended GPS coordinate time series to identify and remove the common mode errors for sites in southern California. *Johannson et al.* [2002] employ empirical orthogonal function analysis to identify and remove correlated noise for GPS sites in Scandinavia. Both techniques proved effective in identifying and removing common mode noise for regional GPS networks.

[66] We estimate and remove common mode noise from the 174 GPS time series employed in our analysis using a stacking technique modified from that described by *Wdowinski et al.* [1997]. Wdowinski et al. solve for a single set of daily common mode corrections for all of their sites, reflecting the relatively small geographical aperture of the southern California GPS network. Given that the GPS sites we use for our analysis span much of the North American plate, we tailored our algorithm to estimate common mode corrections that vary smoothly across the network, thereby capturing any geographic variations in their phase or amplitude.

[67] We estimate the daily common mode corrections for each GPS site as follows: We first do a weighted linear regression of the daily, point-positioned geocentric coordinates of continuous GPS sites in North and Central America and the Caribbean region. The time series of linear residuals for these sites constitute the basis for estimating the common mode component of the noise. Sites with time series shorter than 2 years are excluded from the analysis due to the biasing effect on the residual estimates of seasonal and other longer-period noise [*Blewitt and Lavallée*, 2002]. We exclude daily residual values from a handful of sites that exhibit anomalously high nonlinear motion, including site INEG in central Mexico.

[68] For each of the 160 North American plate and 14 RGNA sites, we construct weighted averages for the north, east, and vertical residual values for each day from 1 January 1993 to 1 March 2003. The weighted average for a selected site includes residual values from all sites within 2000 km of the selected site, but excludes the residual value for the selected site. Each of the residual values incorporated into the weighted average is assigned a weight that depends on the product of two factors, the length of the coordinate time series from which the residual value was derived and the distance to the selected site. The time-dependent weighting factor increases linearly with the length of the time series, reflecting time-dependent improvements in the accuracy of the residual estimates as the effects of seasonal and other noise are averaged down. The distance-dependent weighting factor scales linearly from 1.0 for sites within 500 km of the selected site to zero for sites

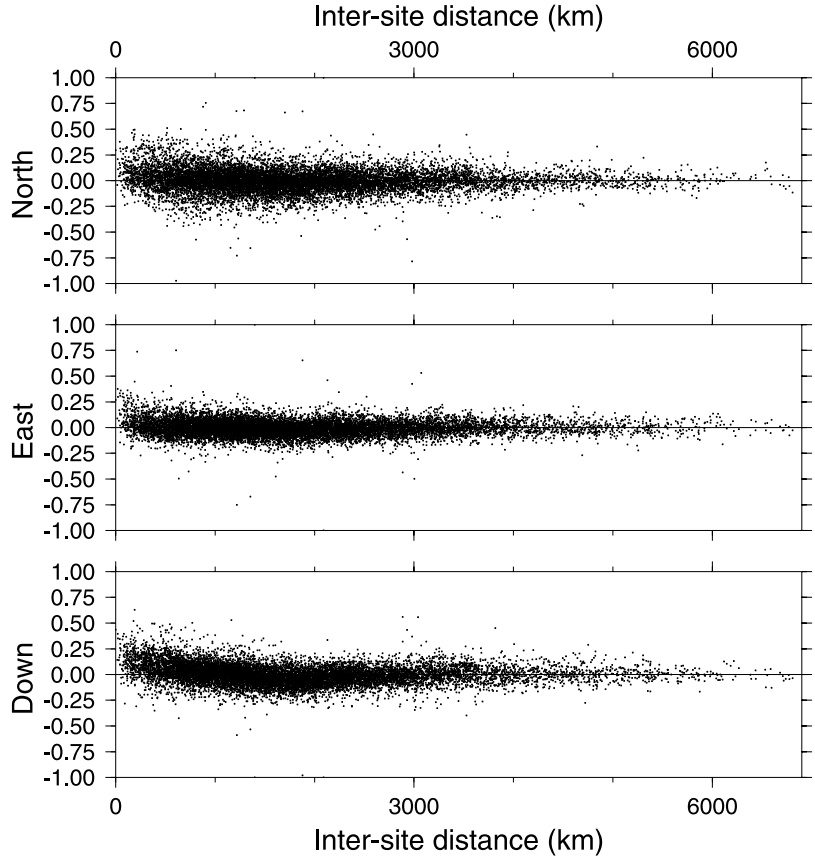

Figure 14. Correlation coefficients between continuous GPS coordinate time series for sites in North America and Mexico after adjusting daily coordinates of all sites for their site-specific common mode corrections (see text) and removing their new best fitting linear trend. Each correlation coefficient is determined from cross correlation of the residual values for two GPS site time series. Site locations are shown in Figure 2.

farther than 2000 km. Residual values for nearby sites with long time series hence contribute significantly more to the weighted average estimate of the common mode noise at a site than do residuals from more distant sites with shorter time series.

[69] Figure 13 illustrates application of this procedure for site MDO1 in Texas. The residual time series for the latitudinal component (Figure 13, top) exhibits daily scatter of 3.5 millimeters before any correction is made for the common mode noise exhibited by sites within 2000 km of MDO1. A weighted stacking of the daily residual values for continuous GPS sites within 2000 km of MDO1 (excluding those for MDO1) yields a time series of daily common mode corrections (Figure 13, middle) that is strongly correlated to the uncorrected residual time series for MD01. Following application of the common mode corrections to the MDO1 daily site coordinates and linear regression of the modified site coordinates, the adjusted residual time series at MD01 (Figure 13, bottom) exhibits daily scatter of 1.7 millimeters in the north component, smaller by a factor of 2.

[70] Applying the above procedure to each of the 174 sites and cross-correlating their modified time series of linear residuals yields cross-correlation coefficients that cluster strongly around zero for all intersite distances (Figure 14). Our procedure thus effectively decorrelates the noise between sites. The reduction in the cumulative variance of the 174 residual time series after applying their daily common mode corrections is 52%, 29%, and 29% for the north, east, and vertical components, respectively, corresponding to average daily scatter of 2.3, 4.5, and 8.1 mm in the north, east, and vertical components. Most of the remaining variance in the corrected residual time series consists of random and long-period noise specific to the site.

[71] The GPS site velocities are also more coherent after we make common mode corrections at each site and re-derive the best fitting site velocities. Least squares inversions of the 160 North American plate site velocities before and after the common mode corrections yield best fitting angular velocities with average misfits of 1.44 and 1.38 mm yr^{-1} to their respective sets of individual site velocities. The common mode corrections thus enhance the signal we are interested in, tectonic motion, relative to the noise contributed by other processes.

[72] The procedure we employ to estimate geographically varying common mode corrections produces a different daily correction for each GPS site, thereby implying we are using the data to estimate many additional parameters (i.e., 174 sites multiplied by 3713, the number of station days). The weighted averaging procedure we use to estimate the common mode corrections guarantees that these param-

eters will be highly correlated between nearby sites given the considerable overlap between the site residuals that are used to estimate the corrections at nearby sites. For example, correlation coefficients between the 174 sets of daily common mode corrections range from 0.9 for many nearby sites to 0.5 for sites thousands of kilometers apart.

[73] Given the high degree of linear dependence between these sets of common mode corrections, we employed singular value decomposition (SVD) of the 174 sets of daily common mode corrections to better estimate the number of linearly independent parameters we are estimating via the weighted stacking procedure. Singular value decomposition of the 174 sets of common mode corrections yields a set of singular values that confirm the high degree of linear dependence between these common mode corrections. The first two singular values describe 95% of the variance within the common mode corrections, thereby indicating that they consist of relatively few linearly independent terms. The notable reduction in the data variance is hence achieved by estimating relatively few additional parameters from the numerous GPS coordinate time series.

[74] We also applied SVD to the 174 residual coordinate time series before any common mode corrections. The first three singular values reduce the variance in the unmodified time series by 45%, after which further reductions in the variance are achieved by 171 small, similarly sized singular values. The first three singular values contain most of the information about the common mode noise and hence reduce the overall variance rapidly. The 171 remaining singular values largely contain information about noise specific to each GPS site and hence reduce the remaining variance more slowly and by small, nearly equal amounts. Overall, ~90% of the common mode component of the noise can be removed via application of two linearly independent sets of corrections.

[75] The above technique for estimating and removing common mode noise can be applied to a global-scale network, provided that GPS sites are sufficiently close to enable regionally averaged common mode noise estimates.

[76] **Acknowledgments.** We thank the employees of INEGI who invested numerous hours extracting the data we requested from old magnetic tapes located at on-site archives. We thank officials at INEGI for providing us with no-cost access to the proprietary GPS data and officials at the Universidad de Guadalajara for assisting in the legal domain and providing significant funding for travel expenses. We thank Ralph Glaus and Geoff Blewitt, who played key roles in developing some of the GPS data processing strategies we employed, and Wallis Hutton for assistance in handling data in the early stages of the project. We thank Tim Masterlark for making the viscoelastic calculations and the GPS group at the Jet Propulsion Laboratory for providing GPS products and software essential for this work. We thank Javier Pacheco-Alvarado, head of the Mexican National Seismic Network and Casiano Jimenez-Cruz, technical operator for providing us with epicentral information. Finally, we thank Richard Bennett, Kurt Feigl, and Isabelle Manighetti for constructive reviews. This work was funded by the Universidad de Guadalajara and National Science Foundation grant EAR-9804905, including a component from NSF International. All graphics were produced using Generic Mapping Tools software [*Wessel and Smith*, 1991].

References

Bennett, R. A., W. Rodi, and R. E. Reilinger, Global Positioning System constraints on fault slip rates in southern California and northern Baja, Mexico, *J. Geophys. Res.*, *101*, 21,943–21,960, 1996.

Bennett, R. A., J. L. Davis, and B. P. Wernicke, Present-day pattern of Cordilleran deformation in the western United States, *Geology*, *27*, 371–374, 1999.

Bennett, R. A., J. L. Davis, J. E. Normandeau, and B. P. Wernicke, Space geodetic measurements of plate boundary deformation in the western U. S. cordillera, in *Plate Boundary Zones*, *AGU Geodyn. Ser.*, vol. 30, edited by S. Stein and J. T. Freymueller, pp. 27–55, AGU, Washington, D. C., 2002.

Blewitt, G., and D. Lavallée, Effect of annual signals on geodetic velocity, *J. Geophys. Res.*, *107*(B7), 2145, doi:10.1029/2001JB000570, 2002.

Bryant, W. R., J. Antoine, M. Ewing, and B. Jones, Structure of the Mexican continental shelf and slope, Gulf of Mexico, *Am. Assoc. Pet. Geol. Bull.*, *52*, 1204–1228, 1968.

Buffler, R. T., F. J. Shaub, J. S. Watkins, and J. L. Worzel, Anatomy of the Mexican Ridges, southwestern Gulf of Mexico, *Mem. Am. Assoc. Pet. Geol.*, *29*, 319–327, 1979.

Burbach, G. V., C. Frolich, W. D. Pennington, and T. Matumoto, Seismicity and tectonics of the subducted Cocos plate, *J. Geophys. Res.*, *89*, 7719–7735, 1984.

Chael, E. P., and G. S. Stewart, Recent large earthquakes along the Middle America Trench and their implications for the subduction process, *J. Geophys. Res.*, *87*, 329–338, 1982.

DeMets, C., A new estimate for present-day Cocos-Caribbean plate motion: Implications for slip along the Central American volcanic arc, *Geophys. Res. Lett.*, *28*, 4043–4046, 2001.

DeMets, C., and T. Dixon, New kinematic models for Pacific-North America motion from 3 Ma to present, 1: Evidence for steady motion and biases in the NUVEL-1A model, *Geophys. Res. Lett.*, *26*, 1921–1924, 1999.

DeMets, C., and D. S. Wilson, Relative motions of the Pacific, Rivera, North American, and Cocos plates since 0.78 Ma, *J. Geophys. Res.*, *102*, 2789–2806, 1997.

DeMets, C., P. E. Jansma, G. S. Mattioli, T. H. Dixon, F. Farina, R. Bilham, E. Calais, and P. Mann, GPS geodetic constraints on Caribbean-North America plate motion, *Geophys. Res. Lett.*, *27*, 437–440, 2000.

Dixon, T. H., A. Mao, and S. Stein, How rigid is the stable interior of the North American plate?, *Geophys. Res. Lett.*, *23*, 3035–3038, 1996.

Dixon, T., F. Farina, C. DeMets, F. Suarez Vidal, J. Fletcher, B. Márquez-Azúa, M. Miller, O. Sanchez, and P. Umhoefer, New kinematic models for Pacific-North America motion from 3 Ma to present: II. Tectonic implications for Baja and Alta California, *Geophys. Res. Lett.*, *23*, 3961–3964, 2000.

Doser, D. I., and J. Rodriguez, The seismicity of Chihuahua, Mexico, and the 1928 Parral earthquake, *Phys. Earth Planet. Inter.*, *78*, 97–104, 1993.

Ferrari, L., V. H. Gaarduño, G. Pasquarè, and A. Tibaldi, Volcanic and tectonic evolution of central Mexico: Oligocene to present, *Geofis. Int.*, *33*, 91–105, 1994.

Gan, W., and W. H. Prescott, Crustal deformation rates in central and eastern U.S. inferred from GPS, *Geophys. Res. Lett.*, *29*, 3733–3736, 2001.

Genrich, J. F., Y. Bock, and R. G. Mason, Crustal deformation across the Imperial fault: Results from kinematic GPS surveys and trilateration of a densely spaced, small-aperture network, *J. Geophys. Res.*, *102*, 4985–5004, 1997.

Gripp, A. E., and R. G. Gordon, Current plate velocities relative to the hotspots incorporating the NUVEL-1 global plate motion model, *Geophys. Res. Lett.*, *17*, 1109–1112, 1990.

Guzmán-Speziale, M., W. D. Pennington, and T. Matumoto, The triple junction of the North America, Cocos, and Caribbean plates: Seismicity and tectonics, *Tectonics*, *8*, 981–997, 1989.

Heflin, M., et al., Global geodesy using GPS without fiducial sites, *Geophys. Res. Lett.*, *19*, 131–134, 1992.

Henry, C. H., and J. Aranda-Gomez, The real southern Basin and Range: Mid- to late Cenozoic extension in Mexico, *Geology*, *20*, 701–704, 1992.

Hutton, W., C. DeMets, O. Sanchez, G. Suarez, and J. Stock, Slip kinematics and dynamics during and after the 1995 October 9 M_w = 8.0 Colima-Jalisco earthquake, Mexico, from GPS geodetic constraints, *Geophys. J. Int.*, *146*, 637–658, 2001.

Johansson, J. M., et al., Continuous GPS measurements of postglacial adjustment in Fennoscandia 1. Geodetic results, *J. Geophys. Res.*, *107*(B8), 2157, doi:10.1029/2001JB000400, 2002.

Johnson, C. A., and C. G. A. Harrison, Neotectonics in central Mexico, *Phys. Earth Planet. Inter.*, *64*, 187–210, 1990.

Kogan, M. G., G. M. Steblov, R. W. King, T. A. Herring, D. I. Frolov, S. E. Egorov, V. Y. Levin, A. Lerner-Lam, and A. Jones, Geodetic constraints on the rigidity and relative motion of Eurasia and North America, *Geophys. Res. Lett.*, *27*, 2041–2044, 2000.

Langbein, J., and H. Johnson, Correlated errors in geodetic time series: Implications for time-dependent deformation, *J. Geophys. Res.*, *102*, 591–604, 1997.

Mao, A., C. G. A. Harrison, and T. H. Dixon, Noise in GPS coordinate time series, *J. Geophys. Res.*, *104*, 2797–2816, 1999.

Márquez-Azúa, B., C. DeMets, and T. Masterlark, Strong interseismic coupling, fault afterslip, and viscoelastic flow before and after the Oct. 9,

1995 Colima-Jalisco earthquake: Continuous GPS measurements from Colima, Mexico, *Geophys. Res. Lett.*, *29*(8), 1281, doi:10.1029/2002GL014702, 2002.

Masterlark, T., C. DeMets, H. Wang, O. Sanchez, and J. Stock, Homogeneous vs heterogeneous subduction zone models: Coseismic and postseismic deformation, *Geophys. Res. Lett.*, *28*, 4047–4050, 2001.

McClusky, S. C., S. C. Bjornstad, B. H. Hager, R. W. King, B. J. Meade, M. M. Miller, F. C. Monastero, and B. J. Souter, Present-day kinematics of the eastern California shear zone from a geodetically constrained block model, *Geophys. Res. Lett.*, *28*, 3369–3372, 2001.

Minster, J. B., T. H. Jordan, P. Molnar, and E. Haines, Numerical modeling of instantaneous plate tectonics, *Geophys. J. R. Astron. Soc.*, *36*, 541–576, 1974.

Okada, Y., Surface deformation due to shear and tensile faults in a half-space, *Bull. Seismol. Soc. Am.*, *75*, 1135–1154, 1985.

Pacheco, J. F., L. R. Sykes, and C. H. Scholz, Nature of seismic coupling along simple plate boundaries of the subduction type, *J. Geophys. Res.*, *98*, 14,133–14,159, 1993.

Pardo, M., and G. Suarez, Shape of the subducted Rivera and Cocos plates in southern Mexico: Seismic and tectonic implications, *J. Geophys. Res.*, *100*, 12,357–12,374, 1995.

Pasquarè, G., V. H. Garduño, A. Tibaldi, and M. Ferrari, Stress pattern evolution in the central sector of the Mexican volcanic belt, *Tectonophysics*, *146*, 353–364, 1988.

Pew, E., Seismic structural analysis of deformation in the southern Mexican Ridges, M. S. thesis, 102 pp., Univ. of Tex. at Austin, Austin, 1982.

Ponce, L., R. Gaulon, G. Suárez, and E. Lomas, Geometry and state of stress of the downgoing Cocos plate in the Isthmus of Tehuantepec, Mexico, *Geophys. Res. Lett.*, *19*, 773–776, 1992.

Rosencrantz, E., Structure and tectonics of the Yucatan basin, Caribbean sea, as determined from seismic reflection studies, *Tectonics*, *9*, 1037–1059, 1990.

Soler-Arechalde, A. M., and J. Urrutia Fucugauchi, Regional rigid-block rotation, small domain rotations, and distributed deformation within the Acambay graben, central Trans-Mexican volcanic belt: Paleomagnetic implications, *Geofis. Int.*, *33*, 565–574, 1994.

Spencer, J. E., and W. Normark, Tosco-Abreojos fault zone: a Neogene transform plate boundary within the Pacific margin of Baja California, *Geology*, *7*, 554–557, 1979.

Stein, S., and R. G. Gordon, Statistical tests of additional plate boundaries from plate motion inversions, *Earth Planet. Sci. Lett.*, *69*, 401–412, 1984.

Stewart, J. H., et al., Map showing Cenozoic tilt domains and associated structural features, western North America, in *Accommodation Zones and Transfer Zones: The Regional Segmentation of the Basin and Range Province*, edited by J. E. Faulds and J. H. Stewart, *Spec. Pap. Geol. Soc.*, *323*, 1998.

Suárez, G., and O. Sánchez, Shallow depth of seismogenic coupling in southern Mexico: Implications for the maximum size of earthquakes in the subduction zone, *Phys. Earth Planet. Inter.*, *93*, 53–61, 1996.

Suter, M., Orientational data on the state of stress in northeastern Mexico as inferred from stress-induced borehole elongations, *J. Geophys. Res.*, *92*, 2617–2626, 1987.

Suter, M., The historical seismicity of northeastern Sonora and northwestern Chihuahua (28–32°N, 106–111°W), *J. S. Am. Earth Sci.*, *14*, 521–532, 2001.

Suter, M., and J. Contreras, Active tectonics of northeastern Sonora, Mexico (southern Basin and Range province) and the 3 May 1887 M_w 7.4 earthquake, *Bull. Seismol. Soc. Am.*, *92*, 581–589, 2002.

Suter, M., M. López Martínez, O. Quintero Legorreta, and M. Carrillo Martínez, Quaternary intra-arc extension in the central Trans-Mexican volcanic belt, *Geol. Soc. Am. Bull.*, *113*, 693–703, 2001.

Urrutia-Fucugauchi, J., and H. Böhnel, Tectonics along the Trans-Mexican volcanic belt according to paleomagnetic data, *Phys. Earth Planet. Inter.*, *52*, 320–329, 1988.

Van Dam, T., J. Wahr, P. C. D. Milly, A. B. Shmakin, G. Blewitt, D. Lavallee, and K. M. Larson, Crustal displacements due to continental water loading, *Geophys. Res. Lett.*, *28*, 651–654, 2001.

Wang, H. F., *Theory of Linear Poroelasticity with Applications to Geomechanics and Hydrogeology*, 287 pp., Princeton Univ. Press, Princeton, N. J., 2000.

Wang, K., J. He, H. Dragert, and T. S. James, Three-dimensional viscoelastic interseismic deformation model for the Cascadia subduction zone, *Earth Planets Space*, *53*, 295–306, 2001.

Ward, S. N., Pacific-North America plate motions: New results from very long baseline interferometry, *J. Geophys. Res.*, *95*, 21,965–21,981, 1990.

Wdowinski, S., Y. Bock, J. Zhang, P. Fang, and J. Genrich, Southern California Permanent GPS Geodetic Array: Spatial filtering of daily positions for estimating coseismic and postseismic displacements induced by the 1992 Landers earthquake, *J. Geophys. Res.*, *102*, 18,057–18,070, 1997.

Wessel, P., and W. H. F. Smith, Free software helps map and display data, *Eos Trans. AGU*, *72*, 441, 445–446, 1991.

Zumberge, J. F., M. B. Heflin, D. C. Jefferson, M. M. Watkins, and F. H. Webb, Precise point positioning for the efficient and robust analysis of GPS data from large networks, *J. Geophys. Res.*, *102*, 5005–5017, 1997.

C. DeMets, Department of Geology and Geophysics, University of Wisconsin-Madison, 1215 W. Dayton St., Madison, WI 53706, USA. (chuck@geology.wisc.edu)

B. Márquez-Azúa, Departamento de Geografía y Ordenación Territorial, Universidad de Guadalajara, Av. de los Maestros y Mariano Barcena, Planta Alta, Guadalajara, Jalisco, México. (bmarquez@udgserv.cencar.udg.mx)